JOURNAL OF GEOPHYSICAL RESEARCH: SPACE PHYSICS, VOL. 118, 804–822, doi:10.1002/jgra.50140, 2013

Statistical study of global modes outside the plasmasphere

M. D. Hartinger,[1], V. Angelopoulos,[2], M. B. Moldwin,[1], K. Takahashi,[3] and L. B. N. Clausen[4]

Received 23 August 2012; revised 17 December 2012; accepted 16 January 2013; published 28 February 2013.

[1] Global modes, trapped fast mode magnetohydrodynamic (MHD) waves in the Earth's magnetosphere, may exhibit a monochromatic frequency spectrum even in the presence of a driver with a broadband frequency spectrum; they can in turn drive standing Alfvén waves at discrete frequencies via field line resonance (FLR). Direct observations of global modes are limited to a few case studies due to unique challenges associated with detecting them in situ. In this study, we use electric field, magnetic field, and plasma data from multiple THEMIS spacecraft as well as ground-based observations to identify and characterize global modes outside the nominal plasmapause location. We establish a lower bound of 1.0% for the global mode occurrence rate in the 3–20 mHz frequency range in that region and show that global modes occur more frequently during high-speed solar wind intervals. We also show that global modes with frequency between 10 and 20 mHz occur preferentially in the noon local time sector and are likely driven by processes in the ion foreshock.

Citation: Hartinger, M. D., V. Angelopoulos, M. B. Moldwin, K. Takahashi, and L. B. N. Clausen (2013), Statistical study of global modes outside the plasmasphere, *J. Geophys. Res. Space Physics*, *118*, 804–822, doi:10.1002/jgra.50140.

1. Introduction

[2] The shear Alfvén and fast (compressional) magnetohydrodynamic (MHD) wave modes are coupled in realistic representations of the Earth's magnetosphere [*Radoski*, 1971]. However, when the azimuthal wave number is low but finite, they are only weakly coupled. Several models have shown that waves similar to the decoupled fast mode (found in isotropic plasma) may strongly couple to standing shear Alfvén waves at the field line resonance (FLR) location, where the fast mode frequency matches the Alfvén wave frequency [*Tamao*, 1965; *Chen and Hasegawa*, 1974; *Southwood*, 1974]. Sometimes these fast mode waves may be trapped or radially standing between different boundaries in the Earth's magnetosphere. Known as global modes [*Kivelson et al.*, 1984; *Wright and Rickard*, 1995], these waves have also been referred to generally as fast mode resonance [*Waters et al.*, 2002], and more specifically, depending on the boundary conditions and other parameters chosen for the model, as cavity modes [*Kivelson and Southwood*, 1985], waveguide modes [*Samson et al.*, 1992], tunneling modes [*Zhu and Kivelson*, 1989], or virtual resonance [*Lee*, 1998]. The MHD approximation describes global modes satisfactorily because their typical frequencies are well below the proton gyrofrequency and they have perpendicular wavelengths much larger than a proton gyroradius.

[3] Arrays of ground stations first showed ultra-low frequency (ULF) waves that may have constant monochromatic tones over a large range of latitudes [*Samson and Rostoker*, 1972]. When standing Alfvén waves are excited by an energy source with a broadband frequency spectrum, one would expect a different scenario, frequency change with latitude change [e.g., *Waters et al.*, 1995]. This apparent discrepancy can be resolved by the global mode, which provides a mechanism for frequency selection in the presence of a driver with a broadband frequency spectrum [*Wright and Rickard*, 1995]; the frequency is determined by the dimensions of the magnetospheric cavity and the plasma conditions within it.

[4] A number of numerical models and simulations have demonstrated the suitability of the global mode mechanism for generating monochromatic ULF waves in the Earth's magnetosphere [e.g., *Wright and Rickard*, 1995; *Claudepierre et al.*, 2009]. In only a few case studies, however, could global modes be identified in situ. Although most of the events studied occurred inside the plasmasphere [e.g., *Takahashi*, 2010], a few occurred outside it [*Kivelson et al.*, 1997; *Mann et al.*, 1998; *Eriksson et al.*, 2006; *Hartinger et al.*, 2012]. This paucity of data precludes analysis of global mode behavior (e.g., spatial occurrence, preference for different driving conditions).

All Supporting Information may be found in the online version of this article.

[1]Department of Atmospheric, Oceanic, and Space Sciences, University of Michigan, Ann Arbor, Michigan, USA.
[2]Department of Earth and Space Sciences, UCLA, Los Angeles, California, USA.
[3]Applied Physics Lab, Johns Hopkins University, Laurel, Maryland, USA.
[4]Institute of Geophysics, TU Braunschweig, Braunschweig, Germany.

Corresponding author: M. D. Hartinger, Department of Atmospheric, Oceanic, and Space Sciences, University of Michigan, 2455 Hayward St., Ann Arbor, MI 48109-2143, USA. (mdhartin@umich.edu)

2169-9380/13/10.1002/jgra.50140

[5] Statistical evidence for global modes is mixed. Although statistical analysis of ground observations provides some support for the operation of the global mode mechanism [e.g., *Samson et al.*, 1991], statistical analysis of in situ observations of ULF wave data gives little support for the global mode mechanism and casts doubt on its importance, particularly in the region outside the plasmasphere. For example, when examining spacecraft magnetometer data, *Engebretson et al.* [1986], *Anderson et al.* [1989], and *Anderson and Engebretson* [1995] found no evidence of global modes apart from broadband compressional perturbations. *Anderson* [1993] and *Anderson and Engebretson* [1995] also found that global modes do not play an important role in the excitation of standing Alfvén waves, except potentially in the noon local time sector. *Clausen and Yeoman* [2009] did not find any evidence for persistent frequencies (often referred to as "magic frequencies") which are often presented as evidence for global modes in studies that use ground-based observations. *Zhu and Kivelson* [1991] found that most compressional wave activity in the Pc5 frequency range (2–7 mHz) has phase relationships (thermal and magnetic pressure out of phase) inconsistent with fast mode (global mode) waves. *Lessard et al.* [1999] examined magnetic field data and found that narrowband compressional perturbations occur frequently in the noon magnetosphere; this could be evidence of global modes or of propagating, narrowband compressional waves. *Anderson* [1993], summarizing the results from many statistical studies with data from various spacecraft covering the Pc3–5 frequency range and radial distances from 5 to 15 *Re*, found that global modes were not the major source of compressional wave activity.

[6] *Kivelson et al.* [1997] listed several reasons why so few global mode waves have been observed; one was that they may have very small amplitudes and be difficult to observe, either because they are not within the detection capability of instruments or because they are obscured by larger amplitude waves. Using numerical models, *Waters et al.* [2002] proposed several techniques that may be more effective than previous methods in detecting global modes.

[7] In this study, we use multiple lines of evidence from single and multi-point observations, based on tests proposed by *Waters et al.* [2002] and other previous wave mode identification studies, to identify and characterize an ensemble of global modes. This endeavor was motivated by recent case studies using data from the Time History of Events and Macroscale Interactions (THEMIS) probes, which successfully identified such wave modes [*Takahashi*, 2010; *Hartinger et al.*, 2012]. The THEMIS probes (THA, THB, THC, THD, and THE) have comprehensive instrumentation appropriate for detecting global modes using multiple lines of evidence. Their observations near the magnetic equator during quiet solar minimum conditions also enhance the chances of detecting these wave modes [*Kivelson et al.*, 1997].

2. Instrumentation

[8] For in situ observations, we use data from the five THEMIS probes [*Sibeck and Angelopoulos*, 2008]. For the probes used in this study, the perigee was 1.5 *Re*, the apogee varied from 10 to 13 *Re*, and the inclination varied from 5° to 12° (an example orbit is shown in Figure 1) [*Frey et al.*, 2008]. Each spinning probe (3 s spin period) is equipped with a fluxgate magnetometer (FGM) [*Auster et al.*, 2008], an electric field instrument (EFI) [*Bonnell et al.*, 2008], an ion and electron electrostatic analyzer (ESA) [*McFadden et al.*, 2008], and ion and electron solid state telescopes (SST) [e.g., *Turner et al.*, 2012]. ESA measures three-dimensional particle distributions and moments (electrons 5 eV–30 keV, ions 5 eV–25 keV) once per spin. SST measures the three-dimensional particle distributions and moments once per spin and is sensitive to energies above 25 keV.

[9] We used amplitude detection thresholds of 0.18 nT and 0.35 mV/m for ULF magnetic and electric field perturbations, respectively. ULF wave amplitude and phase measurement by EFI is affected by several sources of contamination [*Bonnell et al.*, 2008; *Hartinger et al.*, 2012]. *Hartinger et al.* [2012] discussed contamination sources for EFI and how contaminated intervals can be identified on a case-by-case basis for ULF wave studies. A statistical study such as the present one requires a routine method of identifying and removing contaminated intervals. To that end, we developed quality control flags designed to identify contaminated intervals by comparing the electric field measured by the short (40 m tip to tip) and long (50 m tip to tip) EFI booms (in the spin plane) in the frequency domain. The short boom is usually more strongly affected by sources of contamination than the long boom; agreement between measurements from both booms is a strong indicator of high quality data. The procedure for making this comparison and computing the flags is described in the Supporting Information (Figure S1).

[10] We also use ground magnetometer data from the THEMIS ground-based network [*Russell et al.*, 2008], Canadian Array for Realtime InvestigationS of Magnetic Activity (CARISMA) [*Mann et al.,* 2008], Geophysical Institute Magnetometer Array (GIMA) (http://www.asf.alaska.edu/program/gdc/project/magnetometer), United States Geologic Survey network [*Love and Finn*, 2011], Magnetometer Array for Cusp and Cleft Studies (MACCS) (http://space.augsburg.edu/maccs/about.html), Athabasca University THEMIS UCLA Magnetometer Network (AUTUMN)(http://autumn.athabascau.ca/), and Canadian Magnetic Observatory Network (CANMON) (http://www.geomag.nrcan.gc.ca).

3. Methodology

[11] In this section, we outline our global mode identification procedure and its limitations. The main lines of evidence we use are wave polarization consistent with radially standing electromagnetic waves [*Chi and Russell*, 1998; *Waters et al.*, 2002], significant total pressure perturbations indicating the MHD fast mode [e.g., *Song et al.*, 1994], and multi-point observations indicating globally coherent signals that could not be directly driven by the solar wind [*Anderson and Engebretson*, 1995; *Kepko et al.*, 2002].

3.1. Data Processing

[12] For the initial, automatic selection of global mode events, we analyzed an interval that began on 1 February 2008 and ended on 1 April 2010, and we used data from two THEMIS probes, THA and THE. (Our event selection criteria required electric field data, and these data were

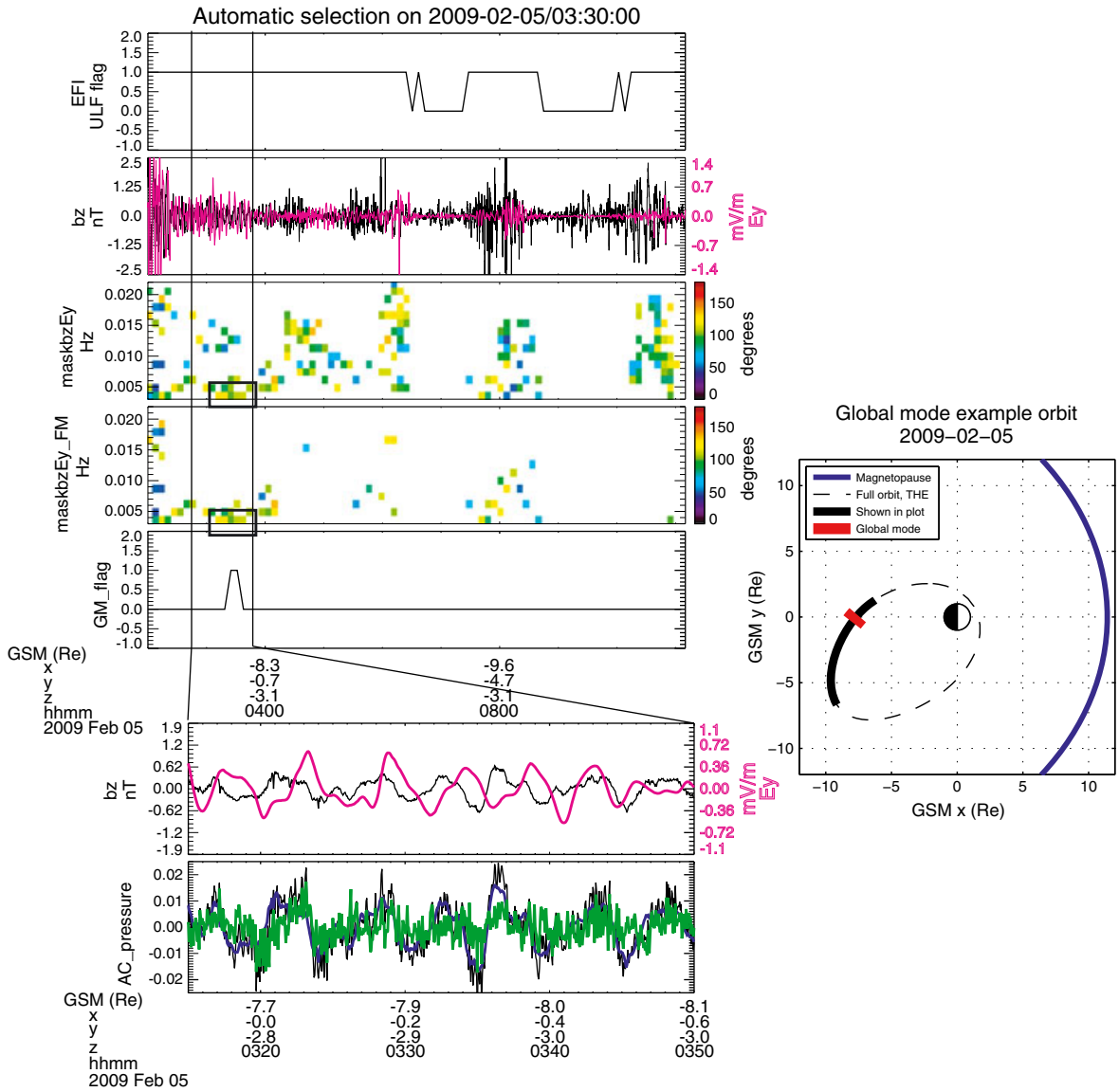

Figure 1. Flag for contaminated electric field data (1 = uncontaminated, 0 = contaminated) (first panel); the magnetic field *z* (black) and electric field *y* (pink) perturbations in nT and mV/m, respectively (second panel); the cross-phase between these perturbations masked where the signal is below the noise threshold and the perturbations are not coherent (coherence $\leq$ 0.7) and their cross-phase is not between 45 and 135 (third panel); the same cross-phase but with an additional mask where none of the tests for fast mode waves are satisfied (fourth panel); and the flag for global modes (1 = global mode, 0 otherwise) (fifth panel). Black boxes mark frequencies/times where at least four consecutive FFT windows met the criteria for automatic selection of global modes. The magnetic field *z* (black) and electric field *y* (pink) perturbations (sixth panel) and the total (black), thermal (green), and magnetic (blue) pressure perturbations for a shorter interval (marked off by black lines) (seventh panel). The inset shows the GSM *xy* view of the entire orbit on 5 February 2009 as a dashed line, the portion of the orbit shown in the main plot as a solid black line, the magnetopause as a blue line, and the portion of the orbit where the global mode was detected as a red line.

not available routinely before January 2008, motivating the choice to begin on 1 February 2008.) The apogee of the THEMIS orbit moves 24 h in local time on a time scale of about 13 months; thus, the apogee moves through all local times twice during the selected interval. We ended our analysis on 1 April 2010 because the THEMIS orbits changed significantly then, with two probes leaving Earth orbit and the other three probes decreasing their typical spatial separations. These new configurations were not ideal for several tests we conducted to validate the automatic global mode selection. Finally, we chose to use THA and THE because they spend more time in the magnetosphere than THB and THC, and THD's orbit is so similar to that of THE that it does not provide much additional data coverage.

[13] To obtain high quality data for these observations and perform EFI diagnostics, fast-survey data are required. This effectively excludes half the THEMIS data set, leaving roughly 800 days of data from both probes (see Supporting Information for fast-survey data coverage, Figure S2). Because of electric field signal contamination by electrostatic wake effects, we also exclude data that are typically in the plasmasphere by restricting our analysis to observations made at distances greater than 5 *Re* from the Earth. Finally, we require that the probe be in the magnetosphere (not in the magnetosheath or solar wind) when making the observations. To remove magnetosheath intervals, we require that the probe be in a region of density less than five particles per cm^3 (further restricting the chances of being in the plasmasphere) and with perpendicular flux (integrated over ESA energies) less than 2×10^7 particles per second per cm^2; through visual inspection of data from several orbits, we found that the density and perpendicular flux were typically elevated above these values in the magnetosheath. For data to be considered in our analysis, all of these criteria must be satisfied for an interval of at least 85 min, the minimum time we require for the removal of background trends and Fourier analysis. We verified that these criteria removed most plasmasphere data and nearly all magnetosheath and solar wind data through visual inspection of magnetic field and plasma data from several randomly selected orbits. With these restrictions, 407 days of data were left.

[14] For all intervals that meet these criteria, we obtain EFI, FGM, ESA, and SST data from the THEMIS website (http://themis.ssl.berkeley.edu/index.shtml) and apply the latest calibrations and corrections using the software package distributed by the THEMIS science team. We remove any gaps and interpolate all data sets to the same time resolution, 3 s. We then check the quality of the electric field data in the spin plane using quality control flags described in the Supporting Information (Figure S1). If the data are contaminated, we exclude them from our analysis. We obtain the component along the spin axis using the $E \cdot B = 0$ approximation, which is devoid of random errors when the normal of the spin plane is at a large angle to the background magnetic field direction. This is normally the case with the THEMIS probes; in all but one global mode event in our final database, the angle is greater than 10° (usually it is greater than 20°). Out of 407 days of fast survey data in the magnetosphere and outside the plasmasphere, there were 135 days of data with uncontaminated electric field data that were above the noise level (see Tables 1 and 2); these are the data we used to search for global modes.

Table 1. Tests for $\beta < 0.5$ Intervals

Test	Discriminator or Confirmation	Available Data (Days)	Passing Data (Days)
EFI	D	194	62.5
$b_z E_y$	D	62.5	< 7.50
Common peak	D	< 7.50	1.97
Not DD	D	N/A[a]	N/A[a]
Multi-sc	C	0.716	0.397
Groundmag	C	0.773	0.598
$P_{th}P_b$	C	1.97	0.782

[a]There are too little data for a meaningful comparison (see section 3.3.1). The solar wind dynamic pressure test was only conducted for seven events, six of which passed.

Table 2. Tests for $\beta \geq 0.5$ Intervals

Test	Discriminator or Confirmation	Available Data (Days)	Passing Data (Days)
EFI	D	213	72.6
$b_z E_y$,$P_{th}P_b$	D	72.6	< 1.81
Common peak	D	< 1.81	0.412
Not DD	D	N/A[a]	N/A[a]
Multi-sc	C	0.260	0.183
Groundmag	C	0.236	0.145

[a]There are too little data for a meaningful comparison (see section 3.3.1). The solar wind dynamic pressure test was only conducted for seven events, six of which passed.

[15] We high-pass filter (frequency > 2 mHz) the electric and magnetic field data and rotate these data into a field-aligned coordinate system in which *z* is along the background magnetic field, *y* points eastward, and *x* completes the right-hand orthogonal set (pointing radially outward at the equator); the background field is obtained by low-pass filtering the magnetic field data (frequency < 2 mHz). We then compute the power spectral density (PSD) of each component of the magnetic and electric field data using a 26 min fast Fourier transform (FFT) window with a three-fourth overlap between windows; a Hanning window is applied to the data before the FFT is conducted. We also calculate the cross-phase and coherence between the *z* component of the perturbation magnetic field and the *y* component of the perturbation electric field. These components are expected to be associated with global modes [*Waters et al.*, 2002]. Before conducting any cross-spectral analysis, we apply a two-point smoothing window in the frequency domain.

[16] We calculate the thermal pressure using ESA and SST ion and electron data, and the magnetic pressure using FGM data. We high-pass filter these pressures, compute the cross-phase between them, and compute the total pressure perturbation. We then calculate the noise threshold associated with the thermal pressure perturbation as a function of frequency and time using Poisson counting statistics from the original ESA and SST measurements. Finally, we obtain the PSD for the thermal, magnetic, and total pressure perturbations. We use these data to identify global modes in the frequency domain, as described in the next two sections.

3.2. Event Selection and Culling I: Single-Point Observations

[17] Global modes, whether they are cavity modes or waveguide modes with small azimuthal wave vector, are observationally similar to radially standing fast mode waves [*Wright*, 1994]. As such, they should have electric field *y* and magnetic field *z* components that are 90° out of phase [*Chi and Russell*, 1998; *Waters et al.*, 2002]. Their thermal and magnetic pressure perturbations should be in phase, however [e.g., *Song et al.*, 1994]. If they are being observed at a location remote from an FLR, they should have significant compressional magnetic field perturbations and east-west electric field perturbations [*Waters et al.*, 2002]. Our initial, automatic event selection criteria were motivated by these features and designed to select intervals with perturbations consistent with radially standing fast mode waves.

[18] To select an event, we first require that the electric field y and magnetic field z perturbations be above the noise thresholds of each instrument and have a coherence greater than or equal to 0.7. In addition, the absolute value of the cross-phase between them must be greater than 45° or less than 135°. These criteria suggest the presence of an electromagnetic wave with a radially standing component [*Chi and Russell*, 1998].

[19] We next determine whether the wave is a fast mode wave using tests designed to find significant total pressure perturbation. The relationship between thermal, magnetic, and total pressure perturbations has been modeled for various wave modes in the Earth's magnetosphere, including the drift-mirror mode [*Hasegawa*, 1969; *Pokhotelov et al.*, 1985], the shear Alfvén (toroidal mode) [*Southwood*, 1977], the compressional Alfvén (poloidal mode) [*Southwood*, 1977], and the drift-compressional Alfvén mode [*Pokhotelov et al.*, 1985]. In all of these wave modes, the thermal pressure perturbation should be out of phase with the magnetic pressure perturbation. In some, the total pressure perturbation should be negligible, whereas in others (e.g., drift-mirror mode), it may be non-negligible but less than the magnetic or thermal pressure perturbation. These relationships have been confirmed through observation [e.g., *Baumjohann et al.*, 1987].

[20] Unlike the above mentioned modes, the fast mode should be associated with significant (exceeding both the magnetic and thermal pressure perturbation) total pressure perturbations and thermal and magnetic perturbations that are in phase [*Song et al.*, 1994]. We seek to discriminate fast mode waves from all other wave modes. When the thermal pressure perturbation is detectable (above noise threshold), one of two conditions must be met for wave activity to be considered a fast mode: (1) the total pressure perturbation must be greater than the magnetic and thermal pressure perturbations or (2) the cross-phase between the thermal and magnetic pressures must be less than 90°. When the thermal pressure perturbation is not detectable (below noise threshold), we require that the wave be compressional: the ratio of the sum of the x and y components of the magnetic field PSD to the z component must be less than one. This second test was used only in a small number of very low β intervals. During these intervals, only the MHD fast and shear Alfvén modes are expected to be present, with the Alfvén mode expected to have primarily transverse magnetic field perturbations near the magnetic equator. Non-global mode events however could be selected using these criteria; therefore, when the thermal pressure perturbation is not detectable, we require additional lines of evidence, described in section 3.3, to select a global mode event.

[21] We conduct tests in the frequency domain using Fourier analysis. Although the accuracy of Fourier analysis in capturing the true nature of time-variable wave activity in space plasmas is limited [e.g., *Paschmann and Daly*, 2000], it can be increased by using multiple FFT windows. To reduce the chances of selecting events that may match our global mode selection criteria because of the uncertainty inherent in the Fourier analysis (e.g., noise with a broadband frequency spectrum), we require our criteria to be met at the same frequency for at least four consecutive FFT windows. Despite the three-fourth window overlap used in our analysis, the first and last of the four FFT windows contain practically independent measurements due to the application of a Hanning function (see section 3.1), which suppresses the signal at the beginning and end of each window.

[22] For this analysis, we only consider the 3–20 mHz frequency band. The 3–20 mHz frequency band is appropriate for this study because several previous observations, simulations, and models of global modes in this region found frequencies within or very close to this frequency range [e.g., *Lee and Lysak*, 1989; *Claudepierre et al.*, 2009]. The lower frequency cutoff at 3 mHz was chosen to exclude ULF waves that may be driven directly by the solar wind; it is difficult to differentiate these waves from global modes. Because of the decreasing precision of our 26 min FFT window in identifying spectral features at higher frequencies, the upper frequency cutoff was chosen. These tests could be repeated at higher frequencies with a different FFT window, but we leave that as a topic for future work.

[23] In Figure 1, we show an example event selection interval. The electric field data were uncontaminated during the beginning of the interval, as indicated by the ULF electric field quality control flag in the first panel. ULF perturbations are seen in both electric field y (black) and magnetic field z (pink) components in the second panel. The third panel shows the cross-phase between these two components. The dynamic cross-phase spectrum has been masked at frequencies/times when the signal is below the noise threshold of either EFI or FGM, the coherence between the two perturbations is less than or equal to 0.7, or the cross-phase between the two perturbations is less than 45° or greater than 135°. It has also been masked when the electric field data are contaminated (note the correspondence between large periods of missing data in this panel and the quality control flag in the first panel).

[24] An additional mask applied to the data in the fourth panel removes all frequencies/times that did not pass the fast mode test, resulting in the data in the fifth panel. In one interval, there are at least four consecutive FFT windows at a constant frequency in which data remain unmasked. These data have been automatically identified as a global mode, as indicated by the flag in the fifth panel. That these data are consistent with the global mode event selection criteria is further demonstrated in the smaller time range in the sixth and seventh panels. In the sixth panel, wave activity is shown with the electric field y (pink) and magnetic field z (black) perturbations 90° out of phase. In the seventh panel, the total (black), thermal (green), and magnetic (blue) pressure perturbations are shown. They are all in phase, and the total pressure changes as expected for a fast mode wave.

[25] We identified many events such as the one shown in Figure 1. We removed the subset of these events that exhibited a broadband frequency spectrum as follows. Interested in only events that can unambiguously be identified as global modes, we removed those in which either the electric or magnetic perturbation exhibited a broadband frequency spectrum. We conducted two tests: an automated examination of the power spectrum and a visual inspection of each signal and the associated cross-phase, coherence, and power spectral densities. For both tests, we required that the power spectral density for the magnetic field z and electric field y perturbations peak at the frequency and time automatically identified as a global mode. An example of this test is shown in Figure 2. The electric field y (pink) and magnetic field

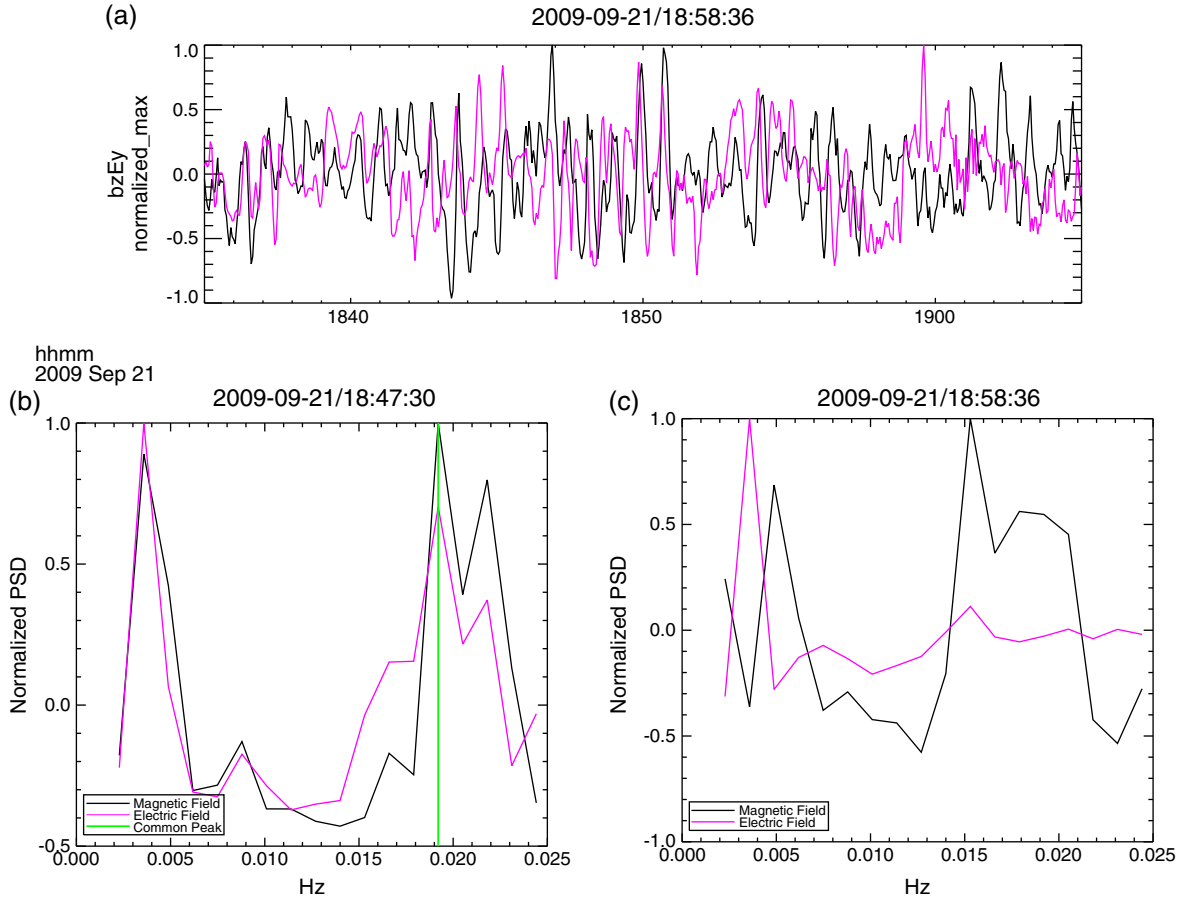

Figure 2. (a) Magnetic field *z* (black) and electric field *y* (pink) perturbations observed during an automatically identified global mode event. (b) The power spectral density with background trend (power law) removed for the magnetic field *z* (black) and electric field *y* (pink) perturbations at 18:47:30 UT, a time chosen with visual inspection. The green line indicates a frequency with a common spectral peak. Clear peaks at 4 mHz were not chosen as common spectral peaks because wave activity at this frequency did not meet the global mode selection criteria. (c) The power spectral density with background trend (power law) removed for the magnetic field *z* (black) and electric field *y* (pink) perturbations for an FFT window at a later time; here, the criteria for a common spectral peak are not met at the expected frequency for the global mode (19 mHz).

z (black) perturbations are shown for an interval when a global mode was detected in Figure 2a. Figures 2b and 2c are for power spectra for each component at two different times. The green line in Figure 2b indicates that a peak in power was seen in both the electric and magnetic field at 19 mHz, the frequency at which a global mode was detected (note that a green line is not shown at 4 mHz because the perturbations at that frequency did not meet the single spacecraft criteria for a global mode): this event passes the common spectral peak test. During the later period shown in Figure 2c, there is not a common spectral peak at 19 mHz and the event does not pass the test at this time. As we conducted the common spectral peak test, we also removed non-unique global mode events from our analysis. (We define a unique global mode event as one that does not occur within 15 min of another global mode event; thus, it must be separated from other events by at least two consecutive FFT windows.)

[26] After automatic selection and culling through visual and automatic inspection of power spectral density peaks, we had identified 93 unique events that passed all tests. Twenty-nine were identified by THA, and 64 were identified by THE. To further reduce the chance of identifying non-global mode events, we then performed three additional tests based on multi-point observations.

3.3. Event Selection and Culling II: Multi-Point Observations

3.3.1. Solar Wind Observations

[27] In section 3.2, we intentionally excluded events that may have been directly driven by the solar wind because the magnetosphere is not expected to respond to the solar wind quasi-statically at frequencies above 3 mHz [e.g., *Kepko and Spence*, 2003]. Thus, part of the motivation for choosing 3 mHz as a lower frequency cutoff was to avoid contamination of our global mode dataset by directly driven waves. There is some recent observational evidence, however, that the solar wind can directly drive ULF waves in the magnetosphere with frequencies as high as 5 mHz [*Viall et al.*, 2009].

Since this falls within the range of frequencies examined in this study, we conduct the following analysis to estimate how many global mode events in the frequency range below 5 mHz could be directly driven.

[28] In seven events in our database, THA or THE identified a global mode with a frequency below 5 mHz while another THEMIS probe (THB or THC) was located in the pristine solar wind (i.e., not in the ion foreshock, magnetosheath, or magnetosphere). We performed a 52 min FFT on the solar wind density, solar wind dynamic pressure, and b_z perturbation associated with the magnetospheric global mode. Time delays caused by propagation of the solar wind from THEMIS probes to the subsolar point were typically less than 1 min, very small compared to the size of the 52 min FFT window we used, so we do not correct for them.

[29] We performed a least squares fit to a power law function for each power spectrum, and then subtracted this power law from the original spectrum to identify peaks more clearly. Finally, we determined whether the event was directly driven by comparing the power spectra of the three signals. If either the solar wind dynamic pressure or density had a common spectral peak with the magnetic perturbation (peaks within 1.3 mHz of each other as determined by visual inspection, same as in section 3.2), we identified that event as directly driven.

[30] An example of this test is shown in Figure 3. Figure 3a, from top to bottom, shows the solar wind dynamic pressure at THC (in the solar wind), solar wind density at THC, and magnetic field z perturbation at THE (in the magnetosphere). An approximately 10 min period wave is seen at THE from roughly 1640 to 1750; however, it is only seen at THC before 1700 and after 1730. Figure 3b shows the power spectrum at 1721 UT (the time of the global mode event observed at THE) for each perturbation normalized to their respective maximum values. A peak is seen at roughly 2 mHz in the magnetic field z perturbation (blue) but not in the solar wind dynamic pressure (pink) or density (black), indicating that the global mode was not directly driven by the solar wind. However, it is possible that the 2 mHz pulsation in the solar wind observed before 1700 supplied energy to the global mode, which persisted after 1700; indeed, when the power spectra from periods before 1700 UT are examined in the same manner as Figure 3b, we find a common spectral peak in both the solar wind and magnetosphere at 2 mHz.

[31] In one case out of seven, there was a peak in power spectral density in both the global mode b_z perturbation and either the solar wind dynamic pressure or density fluctuations. This result should not be directly compared with that of *Viall et al.* [2009], since they only considered events in the noon local time sector, whereas this test was conducted on events which occurred at all local times. Our sample size is limited, and it is difficult to estimate an occurrence rate of directly driven waves in our ensemble of global mode events. However, because only one of seven events was directly driven, and the majority of our events do not have frequencies below 5 mHz, we do not think that directly driven waves mistakenly identified as global modes would significantly affect the results of this study.

[32] Note that events that fail the above analysis may still be global modes. For example, perturbations in the solar wind may have a monochromatic frequency spectrum with a peak that happens to overlap one or more of the resonant global mode frequencies in the magnetosphere [*Wright and Rickard*, 1995]; in such events, it would be very difficult to differentiate between global modes (a resonant

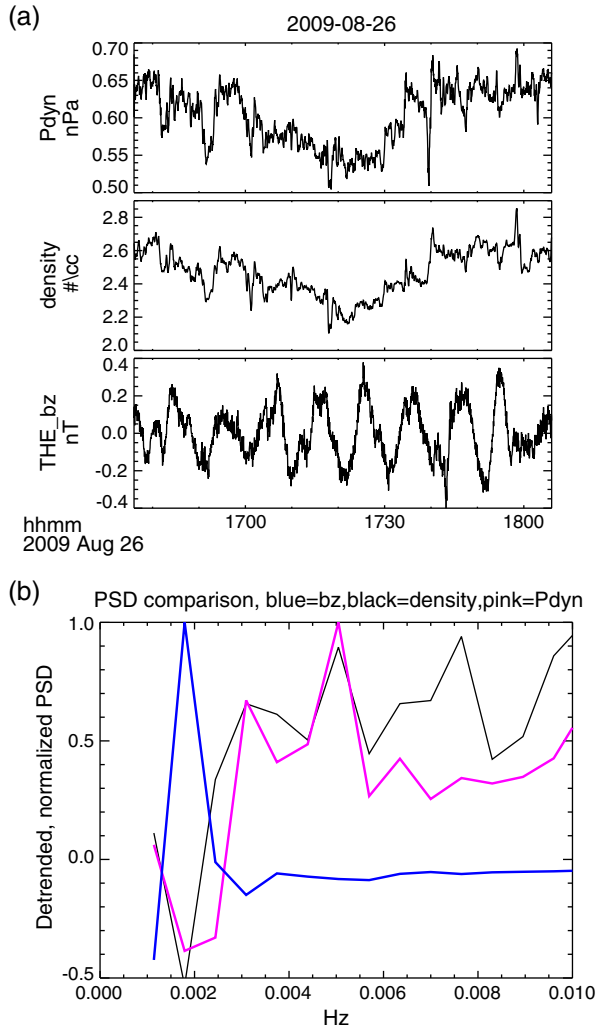

Figure 3. (a) Solar wind dynamic pressure and density measured by THC (which is located in the pristine solar wind), and the magnetic field z perturbation measured by THE in the magnetosphere. (b) A comparison between the power spectral densities at 1721 UT, which have been detrended and normalized to their respective maximum values. Blue is for the magnetic field z perturbation measured by THE, pink is for the solar wind dynamic pressure measured by THC, and black is for the solar wind density measured by THC. There is no corresponding peak in the solar wind for the peak seen in the magnetosphere at roughly 2 mHz, suggesting that this event was not directly driven by monochromatic solar wind fluctuations (although a 2 mHz pulsation observed in the solar wind before 1700 UT may have supplied energy to the global mode). Note this event has a frequency of 2 mHz, which is less than the lowest frequency that we considered in the automatic selection process, 3 mHz. The peak in power associated with the global mode, although at 2 mHz, overlapped enough with that lowest frequency FFT bin (3 mHz) to be identified.

magnetospheric response) and a directly driven, quasi-static magnetospheric response without knowing detailed information about the transit time of fast mode waves in the magnetosphere (to check whether the observed frequency is consistent with a quasi-static response or an accessible global mode frequency).

3.3.2. Multi-Spacecraft Observations

[33] Next, we examined the same global mode events from a multi-probe perspective. We expect global modes to exhibit coherent wave activity over large spatial scales [*Waters et al.*, 2002]. Unlike standing Alfvén waves, which have radial spatial extents of roughly 0.5 *Re* when energy is provided by a monochromatic driver [*Mann*, 1997; *Yeoman et al.*, 1997] and exhibit a continuum of frequencies as radial distance changes [*Anderson et al.*, 1989], global modes should have coherent signals at the same frequency over several *Re* in radial distance. Thus, a test that examines the coherence between signals observed at spatially separated probes could be used to identify and further characterize global modes [*Anderson and Engebretson*, 1995].

[34] For each unique global mode event, we determined whether at least one of the other four THEMIS probes was located at a radial distance greater than 1 *Re* from the observing probe and within the magnetosphere. We computed the coherence between the magnetic field *z* perturbations observed by each spatially separated pair of probes. If any of them had a coherence greater than 0.7, we would consider the signal to be globally coherent, consistent with a global mode.

[35] An example of a global mode event identified by THE that passed the global coherence test is shown in Figure 4. Figure 4a shows the positions of four THEMIS probes, including THE, in the GSM *xy* plane. Figure 4b, from top to bottom, shows the magnetic field *z* and electric field *y* perturbations, an overplot of the band-pass-filtered electric (red) and magnetic (blue) field perturbations, and an overplot of the plasma pressure (green), magnetic pressure (blue), and total pressure (black) perturbations at THE; a global mode was detected at this time, as indicated by the 90° phase relationship between the electric and magnetic field perturbations and the presence of a total pressure

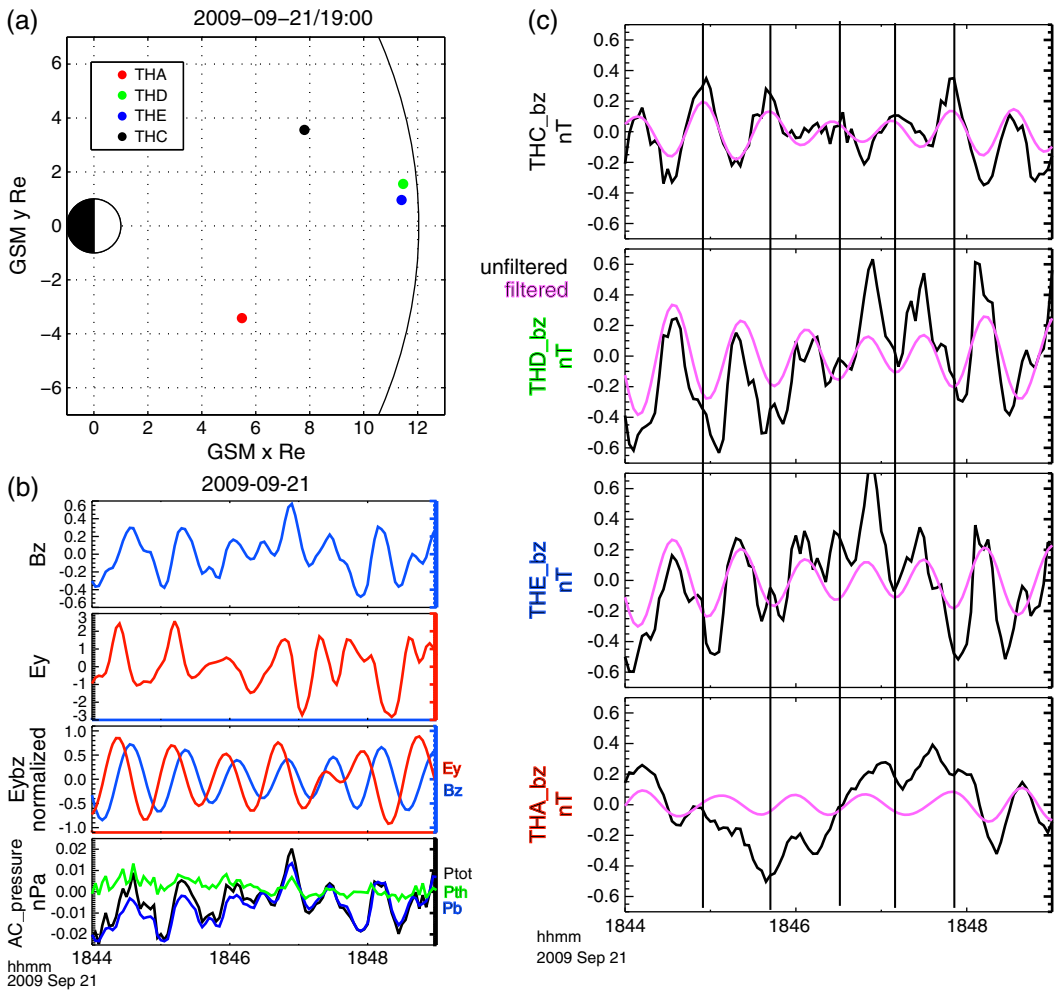

Figure 4. (a) GSM *xy* probe locations. (b) THE observations: the magnetic field *z* and electric field *y* perturbations, an overplot of the band pass filtered electric (red) and magnetic (blue) field perturbations, and an overplot of the plasma pressure (green), magnetic pressure (blue), and total pressure (black) perturbations. (c) the original (black) and filtered (pink) magnetic field *z* perturbations at each probe.

perturbation. Figure 4c shows the original (black) and filtered (pink) magnetic field *z* perturbations at each probe. A roughly 1 min signal is seen at all probes, which have a wide separation in MLT and radial distance; the perturbations are nearly in phase at THD and THE, indicating a low azimuthal wave number as expected for a global mode.

[36] There are several caveats when applying the multi-spacecraft test; most importantly, it is possible for spatially separated probes to be within a global mode, yet not observe coherent signals because one probe is located at a node of the radial standing wave structure. Thus, we could not use this test to exclude events from our database. However, in 35 events in our database, two probes were separated by at least 1 *Re* in radial distance in the magnetosphere, less than 3 h in magnetic local time, and not located near perigee (where wave analysis is not possible). Of these, 24 events (69%) exhibited coherence between probes, indicating that the signals were global and providing additional validation of the event selection in section 3.2. Relaxing these criteria to include larger separations in magnetic local time decreases the number of events exhibiting coherence, as expected for wave activity that is locally excited or affected by dispersion in the magnetospheric waveguide.

[37] For the 24 events that exhibited coherence, we conducted tests on the magnetic field *z* and electric field *y* perturbations to determine if they were coherent and approximately 90° out of phase, as in section 3.2; if the probe that did not originally detect the global mode passes this test, it provides independent confirmation of the global mode event. We do not require fast survey data for these tests (imposing the same requirements as in section 3.2 would substantially reduce the number of events to be tested). Eleven of 24 multi-spacecraft events were independently confirmed by a second probe. In the other 13 events, the other probe may have been located at a node in the electric field perturbation. Alternatively, it is possible that some of these 13 events that were identified as a global mode were actually short-lived superpositions of other ULF wave modes that mimicked the observational signatures of global modes. We discuss this alternative hypothesis more in section 3.4.

3.3.3. Ground Magnetometer Observations

[38] In the third and final type of multi-point analysis, we examined multi-station ground magnetometer data. One of the original observations that led to the development of global mode theories was the detection of monochromatic ground magnetometer pulsations with the same frequency over a wide range of magnetic latitudes corresponding to a wide range of radial distances in the magnetosphere [*Samson and Rostoker*, 1972]. This was unexpected, since different radial distances have different characteristic standing Alfvén wave frequencies; a constant frequency at a wide range of latitudes suggests that some mechanism, such as global modes, imposes a frequency selection. Examination of data from a latitudinal chain of ground magnetometers may thus be one way of testing for the presence of global modes [e.g., *Piersanti et al.*, 2012].

[39] We conducted tests using ground magnetometers in North America, the locations of which are shown in the Supporting Information (see Figure S3). Before beginning the testing, we determined whether the THEMIS probe observing the global mode was conjugate to North America (conjugacy determined using International Geomagnetic Reference Field dipole model). We then computed the coherence between the probe's magnetic field *z* perturbation

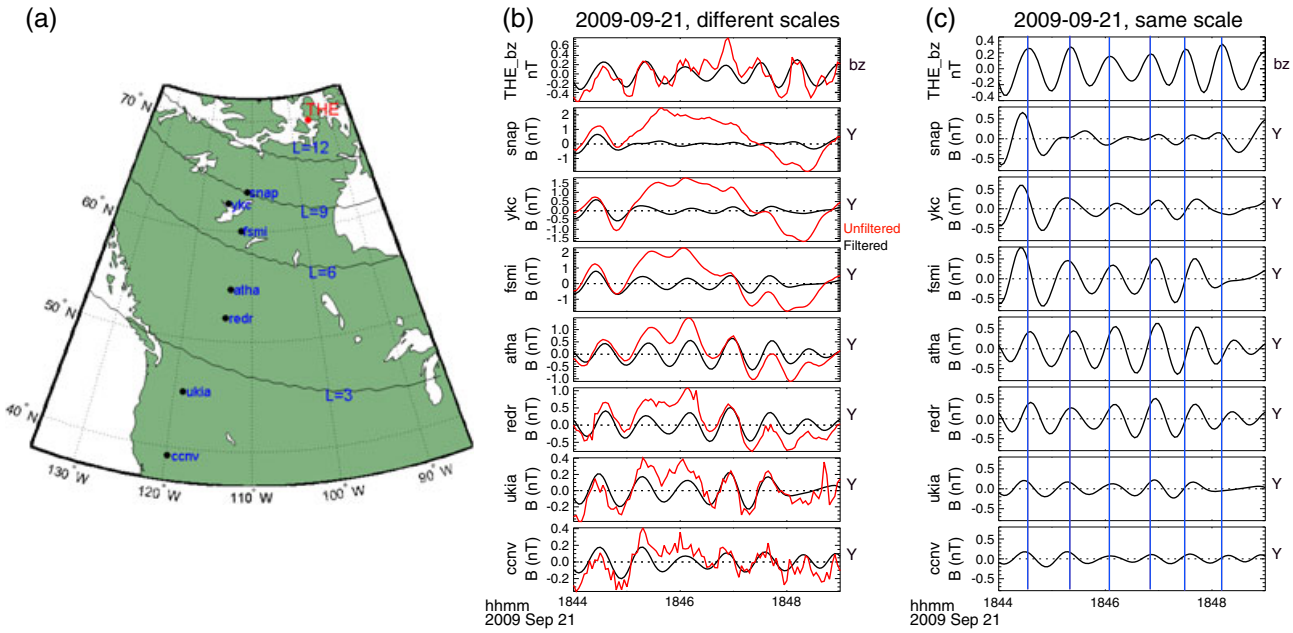

Figure 5. (a) Map of ground magnetometer station locations and the mapped position of THE. (b) The compressional magnetic field perturbation at THE and the east-west magnetic field perturbations at each station from north to south. Red = unfiltered, black = filtered. (c) Same as Figure 5b, with only filtered data on the same scale.

and the east-west component of the magnetic field perturbation observed by all ground stations. Finally, we calculated the mean coherence at the frequency and time corresponding to the global mode observation. If stations separated by more than 5° in magnetic latitude and less than 20° in longitude had signals that were coherent with the global mode signal observed by the THEMIS probe (coherence > 0.7 at the global mode frequency), the event passed the test.

[40] Figure 5 shows an event that passed the test; this is the same event as in Figure 4. The positions of the ground magnetometer stations and the footpoint of THE, the probe that detected the global mode, are shown in Figure 5a. Figure 5b, from top to bottom, shows the magnetic field z perturbation at THE and the east-west magnetic field perturbation at each station; the red traces are the raw data and the black traces are the filtered data. The order of the stations is given by their latitude, with the northernmost station on the top. Figure 5c shows only the filtered data from Figure 5b, with all traces on the same scale. All stations see the approximately 1 min signal; the lack of a significant phase shift precludes the possibility that the ground stations are detecting compressional waves that are propagating inward from the magnetopause (since the transit time would introduce a substantial phase shift over this range of latitudes).

[41] The choice to use the east-west component in these tests was based on numerical models of fast mode propagation from the magnetosphere to the ground which showed that the east-west perturbation can be much larger than the north-south perturbation [*Sciffer et al.*, 2005]. However, the polarization observed on the ground may vary for a variety of reasons independent of the wave polarization in the magnetosphere (e.g., magnetic field dip angle, variations in ionospheric conductivity). To our knowledge, there is no universally agreed upon method for detecting fast mode waves on the ground, particularly at high latitudes; in some cases, the north-south perturbation or total horizontal perturbation may be a better indicator of the presence of global modes, the global mode may only be detectable through the driving of Alfvén waves at the FLR location, or there may be no evidence of the global mode in ground magnetograms [*Kivelson and Southwood*, 1988]. To determine whether the choice to use the east-west magnetic perturbation significantly affected our results, we tried the same tests with the north-south perturbation and total magnetic field perturbation. We found that for nearly all events, events which passed the test using the east-west perturbation also passed using the north-south and total horizontal perturbation.

[42] In 30 events, magnetometers in North America with a separation of at least 5° in magnetic latitude and a separation in longitude of less than 20° observed coherent signals (east-west magnetic field perturbations). In 39 total events, North America was conjugate to the global mode observation; thus, ground observations, when available, confirmed the in situ global mode observation 77% of the time. We do not discard the nine events that failed this test because of the uncertainties involved in observing fast mode wave signatures on the ground [*Kivelson and Southwood*, 1988; *Sciffer et al.*, 2005].

[43] In 26 of the 30 passing global mode events, one or more additional probes were conjugate to North America; we repeated the ground magnetometer test for the other probes in these events (at the global mode frequency), finding that 20 of 26 events had one or more additional THEMIS probes that passed. In other words, a second probe passed the ground magnetometer test 77% of the time.

3.4. Summary of Event Selection and Limitations

[44] We used data from both automatic and visual tests to identify a final list of global mode events. All events must satisfy the following criteria, which are based on single-probe observations at one frequency for at least four consecutive FFT windows (26 min):

[45] 1. Electric field data are uncontaminated and above the noise threshold, so the cross-phase between electric and magnetic field perturbations is trustworthy.

[46] 2. Electric field y and magnetic field z perturbations are above the noise threshold and have a coherence greater than or equal to 0.7.

[47] 3. The absolute value of the cross-phase between these two perturbations is greater than 45° or less than 135°, suggesting a radially standing fast mode wave.

[48] 4. These two perturbations exhibit a monochromatic frequency spectrum and have a common spectral peak.

[49] 5. Wave activity is consistent with fast mode MHD waves. If $\beta < 0.5$, we require that either the magnetic field perturbation is compressional or there is a significant total pressure perturbation (or, equivalently, that the thermal and magnetic pressure perturbations are in phase). If only the former is satisfied, we require that the event pass either the multi-point space or ground observation tests as an additional line of evidence. If $\beta \geq 0.5$, we require a significant total pressure perturbation; if this criterion is not satisfied, we discard the event.

[50] After these tests, we used a solar wind monitor test described in section 3.3.1 to cull one event from our database of 93 events. We also used multi-spacecraft and ground magnetometer tests, described in sections 3.3.2 and 3.3.3, to confirm the presence of global modes (one of these tests must be passed when $\beta \geq 0.5$ or when $\beta < 0.5$ and the thermal pressure perturbation is below the noise threshold). Twenty of 92 events did not pass at least one of these tests, and they were culled. We were left with 72 global mode events for further study in section 4. The time of each of these events are listed in the Supporting Information (Table S1).

[51] Tables 1 and 2 show the amount of data available after each step in the culling process. Each test in the culling process is classified according to whether it is a discriminator (i.e., an event will be discarded if it fails the test) or if it is used as confirmation of a global mode event (i.e., the event will not necessarily be discarded if it fails the test or if the test cannot be conducted). "Available Data" is the number of days of data available for the test to be conducted, and "Passing data" is the number of days of data that passed the test. Table 1 is for the selection process during $\beta < 0.5$ intervals, whereas Table 2 is for $\beta \geq 0.5$ intervals. "EFI" refers to item 1 in the above list (the test also discards data that are below the EFI noise floor), $b_z E_y$ collectively refers to items 2 and 3 in the above list, "Common Peak" refers to item 4, "Not DD" refers to the test discussed in section 3.3.1, "Multi-sc" refers to the test in section 3.3.2, "Groundmag" refers to the test in section 3.3.3, and $P_{th}P_b$ refers to the total pressure perturbation test in item 5 above (a discriminating

test for $\beta \geq 0.5$ intervals and a confirming test for $\beta < 0.5$). The < symbol indicates that some events may have been double counted, leading to an overestimate of the number of days of data.

[52] Our event selection methodology has some important limitations. According to *Wright* [1994], dispersion of fast mode waves in the flank magnetosphere can play an important role in determining the observed signal. *Rickard and Wright* [1995] showed that signals associated with a superposition of waveguide modes with different azimuthal wave vectors are rarely smooth and monochromatic, making it difficult to unambiguously identify waveguide modes or differentiate them from ambient noise. Our study cannot detect a superposition of waveguide modes; discrete waveguide modes with high azimuthal wave number will also be excluded, as they are not radially standing. However, this study will detect waveguide modes that appear as monochromatic, radially standing waves. This can occur when the waveguide modes are being driven by a source in the same local time sector or long after transient driving occurs [*Wright*, 1994].

[53] An additional limitation of this study is that it requires coherent electric and magnetic field perturbations above the noise threshold of the respective instruments. Global modes are nodal structures, and when a spacecraft is located near a node in either the electric or magnetic field, it may not measure a signal above the noise. As such, this study may exclude some global modes during periods when the probes are not appropriately positioned to detect them. Furthermore, it is possible that global modes will not be detected at their peak amplitudes (since electric field nodes correspond to magnetic field anti-nodes, and vice versa). Previous models and simulations predict different minimum amplitudes/spatial extents for the global mode nodes (due to, for example, different assumptions for the plasma mass density distribution, magnetosphere geometry, and energy input); in some models, perturbations at nodes would be detectable with THEMIS instrumentation [e.g., *Claudepierre et al.*, 2009] whereas in others they would not [e.g., *Waters et al.*, 2002]. Given this variability in predictions for nodal structure and amplitude, it is not clear how significantly the THEMIS instrument noise thresholds affect the detection of global modes near nodes.

[54] Finally, a superposition of ULF wave modes could mimic the observational signatures of a global mode. Thus, it is possible that some of the events in our database of events are not global modes. This is more likely to occur when the event duration is very short. It is also more likely when a multi-point observation (ground magnetometer or spacecraft) is not available or does not confirm the single-spacecraft observation of the global mode: it is less likely that a superposition of wave modes would mimic a global mode signature at two points simultaneously (provided the observation points are far enough apart). Out of 72 events, 22 did not pass either the ground magnetometer or multi-spacecraft test and were short in duration ($\leq$26 min, or four FFT windows). These events are the most likely to have been mistakenly identified as global modes. A future study could examine the events in our database (listed in Table S1) in greater detail to better quantify this problem.

[55] Despite the limitations in our study, the majority of events in our final database are global modes. All of the events in our database satisfy the observational selection criteria for global modes described by *Waters et al.* [2002]. Furthermore, we applied several tests in addition to *Waters et al.* [2002] to remove any possibility of selecting non-global mode events, such as mirror mode or compressional Alfvén waves.

4. Statistical Results

[56] In section 3, we identified global mode events using an automated selection technique followed by both automated and visual culling techniques to obtain a list of 72 global mode events. The locations of these events in the GSM *xy* plane are shown as black dots in Figure 6. Data coverage is also shown as color contours; we define each FFT window eligible to be counted as a global mode as an observation. Since four consecutive FFT windows are required to detect a global mode, two FFT windows at the beginning of each fast-survey interval and one at the end of each fast-survey interval are not included as observations. Intervals with contaminated electric field data, those without fast-survey data, those inside 5 *Re* or outside the magnetopause, and those that were too short for the required detrending and Fourier analysis were also not included as observations (see Figure S2 for full fast-survey data coverage).

[57] In the past, supporting statistical evidence for global modes came from ground-based observations [e.g., *Samson et al.*, 1991; *Mathie and Mann*, 2000] and statistical results from in situ observations provided mixed evidence for global modes, with little evidence of the existence/importance of global modes outside the plasmasphere [e.g., *Anderson et al.*, 1989]. In this study, we identified 72 global mode events outside the plasmasphere.

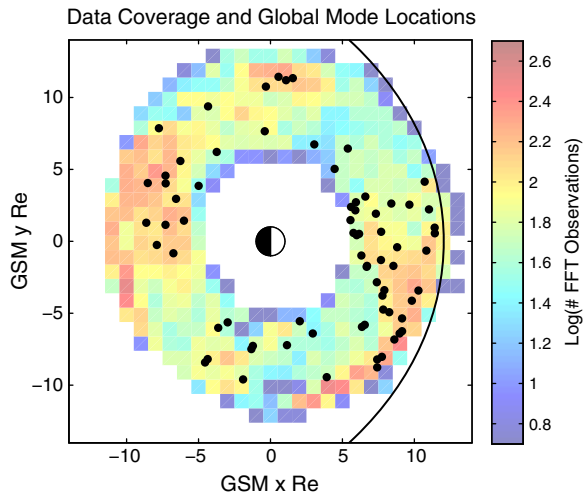

Figure 6. The GSM *xy* view of all global mode events. Each black dot indicates the position of the THEMIS probe in the GSM *xy* plane when it detected a global mode signature. Color contours are for the data coverage. Each observation corresponds to one FFT window and only FFT windows which are eligible to be counted as a global mode are included (i.e., FFT windows at the beginning or end of data intervals and FFT windows with contaminated electric field data are not included).

Many events had very low wave amplitudes compared to other typical sources of ULF wave activity and would be difficult to detect solely through visual inspection of traces or dynamic power spectra, perhaps explaining why so few have been observed in the past. The interval chosen for statistical analysis also had few periods of elevated geomagnetic activity, so there were fewer sources of ULF wave activity that could obscure the presence of global modes.

[58] This is the first study to detect a large number global modes using in situ wave mode identification; as such, it provides strong evidence for the existence of global modes outside the plasmasphere, complementing a small number of previous case studies using in situ observations [*Kivelson et al.*, 1997; *Mann et al.*, 1998; *Eriksson et al.*, 2006; *Hartinger et al.*, 2012]. This ensemble of events can be used to characterize the behavior of global modes in aggregate, gaining additional information to that provided by case studies.

[59] We can obtain a normalized occurrence rate for global modes in different regions and under different driving conditions by determining the length of time (% time) global modes persisted in that region/during those conditions. The total amount of observation time is defined as the total number of observations multiplied by 6.5 min (since 75% of each FFT window overlaps another FFT window, we count each 26 min FFT window as being equivalent to 6.5 min). The total observation time, defined in this manner, including both THA and THE, is 135.07 days.

[60] We define the total duration of global mode events using the start and stop times for each individual global mode event. The total global mode observation time from all 72 events is 1.35 days. We define the overall occurrence rate of global modes (1.0%) as the total global mode observation time divided by the total observation time. We can estimate how this occurrence rate could change if we repeated our observations and used the same event selection methodology during other 26 month periods with similar driving conditions. We must also assume that the same sources of systematic bias would be present in the new sets of observations. From period to period, we would then expect the number of observed global mode events to be well represented by the Poisson distribution. The standard deviation for the number of observed events can then be represented as the square root of 72 (the number of global mode events), 8.49. Assuming that the average duration of global mode events is 1.35 days divided by 72 events, or 0.0188 days, we can obtain a range for the expected occurrence rate of global mode events, from $(1.35 - 0.0188 \times 8.49)/(135.07) \times 100 = 0.881\%$ to $(1.35 + 0.0188 \times 8.49)/(135.07) \times 100 = 1.12\%$. This is an estimate of the random counting error associated with our global mode observations; we reiterate that it does not include sources of systematic error. To our knowledge, this is the first attempt to estimate the occurrence rate of global modes using in situ observations. Several limitations of our methodology would lead to fewer global modes being observed, as discussed in section 3.4. We should thus regard 1.0% as a lower bound for the true occurrence rate of global modes.

[61] In the following sections, we examine the properties of global modes using normalized occurrence rates that depend on spatial position and driving conditions. We also examine whether the frequency of global modes varies as a function of spatial position or driving condition and compare our results to earlier models, simulations, and observations of global modes.

4.1. Favored Locations of Global Modes

[62] Figure 6 indicates that some local time sectors and radial distances are better covered than others, suggesting that the apparent clustering of global mode events at different locations may be misleading. For this reason, we will examine normalized occurrence rates at various locations.

[63] The occurrence rate in various local time sectors, defined in the same manner as the normalized overall occurrence rate, is shown in Figure 7a. The total observation time (hours), total global mode observation time (hours), total number of global mode events, and range for the occurrence rate are shown for each local time sector and defined in the same manner as for the calculation of the overall occurrence rate. The overall occurrence rate is shown as a line in red for reference. Global modes are far more abundant at noon than in all other local time sectors. They are the least abundant at midnight. The dawn and dusk local time sectors have an intermediate occurrence rate.

[64] There are three likely reasons for the local time asymmetry in the global mode occurrence rate. The first is

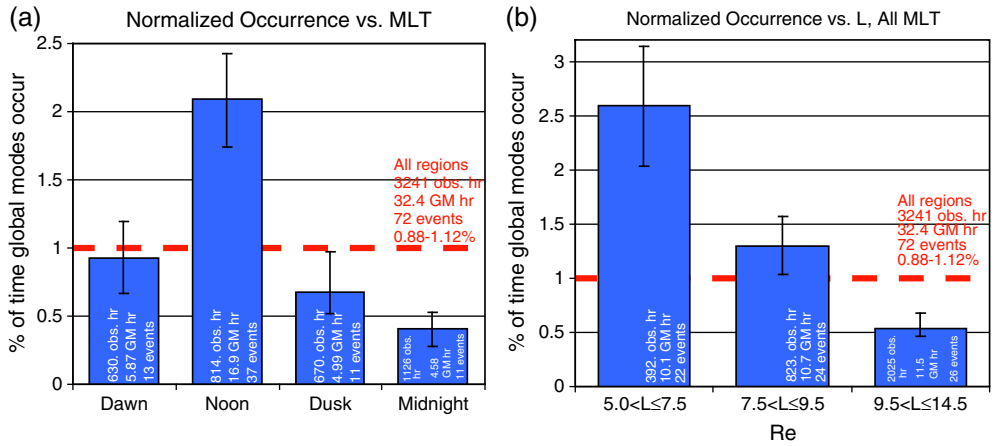

Figure 7. (a) The normalized occurrence rate of global mode events versus MLT. (b) The normalized occurrence rate of global mode events versus L.

that the primary energy sources for global modes are located in the noon sector. This is consistent with previous observations that suggest that the ion foreshock and solar wind dynamic pressure are important drivers of global modes [e.g., *Kivelson et al.*, 1997; *Eriksson et al.*, 2006]. Generally, ion foreshock and solar wind dynamic pressure fluctuations are most effective at driving ULF waves in the noon local time sector [*Takahashi et al.*, 1981; *Takahashi et al.*, 1984; *Takahashi and Ukhorskiy*, 2007].

[65] The second reason for the local time asymmetry of the occurrence rate is the biasing of our study with regard to observing certain waveguide modes. At local noon, assuming a wave energy source that is symmetric with respect to the noon meridian, a superposition of waveguide modes propagating both eastward and westward would be observed. This superposition is observationally similar to a waveguide mode with 0 azimuthal wave vector. The observational signature, which is identical to a monochromatic, radially standing fast mode wave, would be detected during our event selection. In other local time sectors, a superposition of wave modes with a continuum of azimuthal wave vectors would be observed; this superposition would change as a function of time if the driving is transient [*Wright*, 1994]. Such modes may include both azimuthally propagating and radially standing wave behavior farther from noon and may not appear monochromatic. A signature similar to a monochromatic, radially standing fast mode wave would be less likely to be generated or observed [*Rickard and Wright*, 1995]. Thus, our event selection methodology, designed to detect radially standing fast mode waves, is biased to detect global modes close to the noon local time sector.

[66] A third reason for the local time asymmetry is that the magnetospheric cavity/waveguide may not be able to sustain global modes equally well in different local time sectors. This could explain the relatively low occurrence rate for global modes on the nightside, where there is no fixed outer boundary such as the magnetopause to reflect and trap fast mode wave energy. In fact, it is surprising that any radially standing fast mode waves exist in this local time sector, as fast mode wave energy would be expected to rapidly escape into the magnetotail (Figure 1 shows a nightside event). Further examination of the trapping and driving mechanisms of these few nightside events is a topic of future studies.

[67] In Figure 7b, we examine the occurrence rate of global modes as a function of L, or the radial distance at which a dipole magnetic field line crosses the magnetic equatorial plane [*McIlwain*, 1966]. All global modes were observed between L of 5.9 and 12.3 *Re*. The occurrence rate for global modes is highest for low L ($5.9 < L \leq 7.5$) at 2.6%, lower for moderate L ($7.5 < L \leq 9.5$) at 1.3%, and lowest for high L ($9.5 < L \leq 12.3$) at 0.54%.

[68] There are three potential reasons for the dependence of global mode occurrence rate on L. Higher L values are closer to the magnetopause, where wave activity with a broadband frequency spectrum is commonly observed because of transient magnetopause perturbations or waveguide modes with a continuum of azimuthal wave vectors, which appear as wave activity with a broadband frequency spectrum [*Rickard and Wright*, 1995]. Both types of wave activity would tend to obscure monochromatic, radially standing global modes, making it more difficult to identify events in this region. Also, waveguide modes with low azimuthal wave vector are expected to have their turning points at lower L values than waveguide modes with high azimuthal wave vector [*Wright*, 1994]. Thus, only waveguide modes with low azimuthal wave vector would be observed at low L values; a superposition of waveguide modes would be observed at higher L values. These isolated waveguide modes with low azimuthal wave vector are more likely to be identified during the event selection process.

[69] A third reason for the L dependence could be that there is a preferred global mode radial structure. The plasmasphere plays an important role in determining the radial structure of global modes [*Zhu and Kivelson*, 1989; *Lee*, 1998]. The plasmapause is most likely to be located at approximately 4.5 *Re* during the predominately quiet geomagnetic conditions of this study [*Moldwin et al.*, 2002]. The L dependence in the global mode occurrence rate, if interpreted in the context of radial structure, suggests that the region between 5 and 7.5 *Re* (just outside the plasmapause) is where the electric and magnetic perturbations associated with the global mode are easily detectable (whereas at higher L shells they are not). This is consistent with the idea of a persistent global mode trapped within the plasmasphere, with decaying amplitude with increasing distance from the plasmaspause [*Lee and Lysak*, 1999; *Takahashi et al.*, 2003].

4.2. Favored Driving Conditions for Global Modes—Geomagnetic Activity

[70] We obtained hourly geomagnetic activity indices and solar wind data from OMNIweb for use in computing occurrence rates for different driving conditions. The solar wind data were time referenced to the subsolar magnetopause.

[71] We examined the dependence of the global mode occurrence rate on the Kp and AE indices, and we found no strong relationships. The observation interval occurred during solar minimum, however, when the nominal level of geomagnetic activity is expected to be lower. We note that of 72 events, only three occurred during intervals when Kp was greater than or equal to 4 and only 15 occurred during intervals when AE was greater than or equal to 200 nT. This suggests a preference of global modes for lower geomagnetic activity, as suggested by *Kivelson et al.* [1997], but we do not regard it as conclusive evidence because of a paucity of observations during intervals with higher geomagnetic activity. The paucity could also be due to obscuration of global mode signals by other high amplitude ULF waves driven by storms and substorms.

4.3. Favored Driving Conditions for Global Modes—IMF Cone Angle

[72] The ion foreshock is an important energy source for ULF waves in the dayside magnetosphere, particularly during intervals of radial IMF [*Troitskaya et al.*, 1971; *Fairfield et al.*, 1990; *Engebretson et al.*, 1991; *Clausen et al.*, 2009; *Eastwood et al.*, 2011]. Waves originating in the ion foreshock have been suggested as a driver of global modes [*Kivelson et al.*, 1997; *Takahashi*, 2010]. Because the ion foreshock is most effective at generating ULF waves in the magnetosphere during intervals of radial interplanetary magnetic field (IMF), we examine the dependence of the global mode occurrence rate on IMF cone angle. Cone angle values close to 0 or 180° are associated with radial IMF and

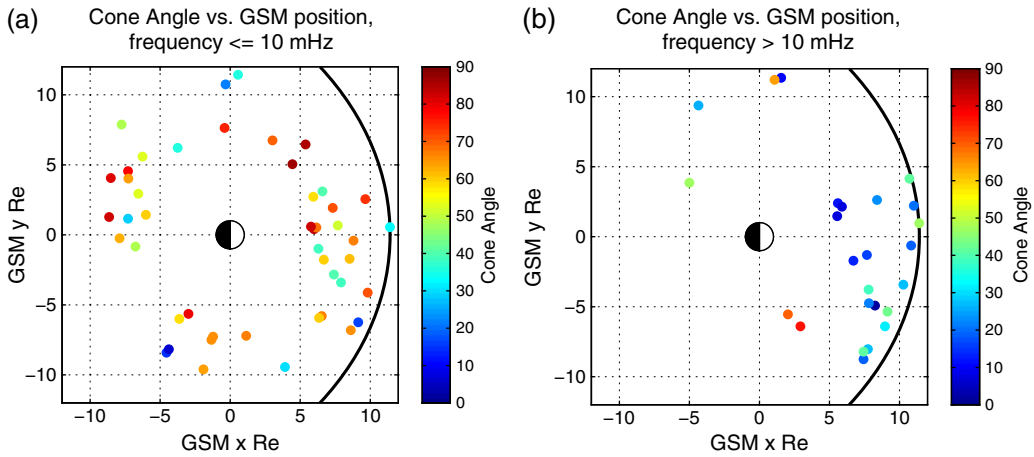

Figure 8. (a) The cone angle of global mode events with frequencies less than or equal to 10 mHz versus GSM *xy* position. To focus on differences between radial and perpendicular (to Earth-Sun line) IMF, we apply the transformation $\theta \rightarrow |180 - \theta|$ when the cone angle is larger than 90°. (b) The same but for frequencies greater than 10 mHz.

intervals of strong driving of magnetospheric ULF waves [*Troitskaya et al.*, 1971]. They would also be associated with a higher occurrence of global modes, if the ion foreshock is an energy source for the global modes.

[73] We found that the normalized occurrence rate for global modes was more elevated during intervals of low cone angle ($0 < \theta \leq 45$), at about 1.5%, than during intervals with higher cone angles. This trend is most evident when the cone angle is plotted versus position for each event and sorted by frequency. In Figure 8a, the cone angle is plotted for all events with frequencies less than or equal to 10 mHz. Here, we only want to differentiate between cases when the IMF is radial and those when the IMF is perpendicular to the Earth-Sun line; we thus transform all cone angles greater than 90° according to $\theta \rightarrow |180 - \theta|$. There is no clear relationship between cone angle and global mode occurrence here, with all events spread throughout the magnetosphere and displaying a wide range of cone angles.

[74] The situation is different in Figure 8b, where the cone angle is plotted for all events with frequencies greater than 10 mHz. First, most events with frequencies greater than 10 mHz are clustered near pre-noon and noon, in contrast to those in Figure 8a. Second, all events in this cluster occurred when the cone angle was either close to 0 or 180°. This evidence strongly suggests that the ion foreshock is the most important source of energy for global modes with frequencies greater than 10 mHz near the noon local time sector. It is consistent with the identified ion foreshock driver in the *Kivelson et al.* [1997] case study in which the wave activity, like the events in Figure 8b, had a frequency above 10 mHz. This evidence is also consistent with earlier observations of magnetospheric ULF waves driven by ULF waves in the ion foreshock occurring most often at these locations and frequencies [*Takahashi et al.*, 1981; *Takahashi et al.*, 1984]. The propagation speed of these ULF waves is less than the bulk flow of the solar wind [e.g., *Burgess*, 1997]; when the cone angle is low and the ion foreshock is near the subsolar point, these waves will impinge on the bow shock and can ultimately provide energy for global modes. Conversely, when the cone angle is larger and the ion foreshock is further from the subsolar point, any ULF wave energy in the ion foreshock will be swept downstream with the bulk flow of the solar wind without affecting the magnetosphere or providing energy for global modes.

4.4. Favored Driving Conditions for Global Modes—Solar Wind Flow Speed

[75] We next examine the dependence of global mode occurrence rate on solar wind flow speed. We expect that the occurrence rate should generally increase with increasing solar wind flow speed. One reason is that more energy is available for global modes during these intervals, either through surface waves generated by flow-shear instabilities, increased fluctuations in the IMF [*Kim et al.*, 2011], or through perturbations originating in the ion foreshock that can affect the magnetosphere during radial IMF conditions (both fluctuations in IMF and radial IMF conditions often occur during intervals of high solar wind speed). Another reason is the change in the nature of the boundary condition at the magnetosheath at high solar wind speed, which can effectively energize global modes [*Mann et al.*, 1999].

[76] Figure 9a shows the dependence of the global mode occurrence rate on solar wind flow speed. We separated the data into two local time regions before computing the occurrence rate. The first region included the dawn and dusk sectors ($3 < MLT \leq 9$ or $15 < MLT \leq 21$). Data for this region are shown in the left two bars in Figure 9a; as expected, the occurrence rate increases from 0.7% to 1.3% as the solar wind velocity increases from $263 < v_{sw} \leq 450$ to $450 < v_{sw} \leq 751$. The second region included the noon sector ($9 < MLT \leq 15$). Data for this region are shown in the right two bars in Figure 9a; here, the occurrence rate also increases, from 1.8% to 3.2%. We do not show data from the midnight sector ($21 < MLT$ or $MLT \leq 3$), as there were too few events to make a significant comparison; however, no correlation between solar wind speed and occurrence was immediately obvious when examining the 11 events found near midnight.

[77] It is unclear from Figure 9a what is causing the occurrence rate to increase at higher solar wind speeds.

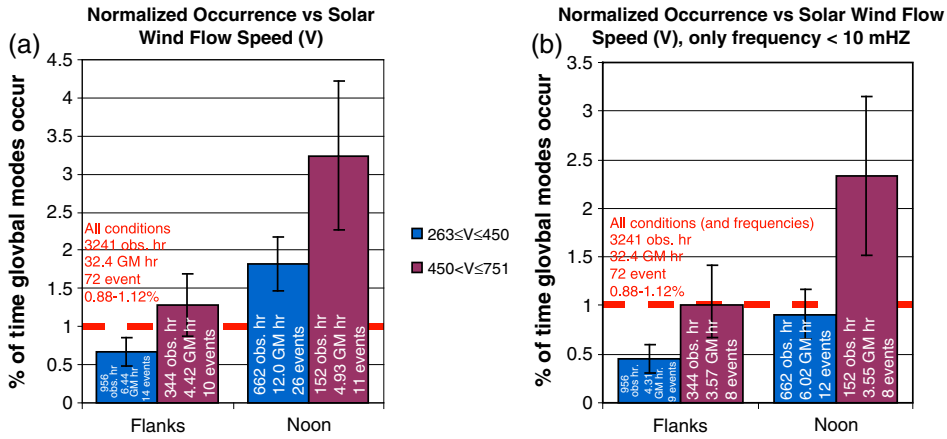

Figure 9. (a) The occurrence rate of global mode events versus solar wind flow speed for all events. The left two bars are for data that includes the dawn and dusk magnetic local time sectors, and the right two bars are for data that includes the noon local time sector. (b) The same as in Figure 9a, but only including events with frequency below 10 mHz.

One possibility is that the increased solar wind speed is correlated with radial IMF conditions, which are ideal for driving ULF waves via processes originating in the ion foreshock. Figure 8 showed that global mode events with frequencies above 10 mHz were strongly correlated with radial IMF conditions, but those with frequencies below 10 mHz had little apparent correlation. In Figure 9b, we present normalized occurrence rates in the same manner as Figure 9a, but we only include events with frequencies below 10 mHz, to determine whether the increase in occurrence at high solar wind speeds is only due to a preference for lower cone angles/radial IMF during these conditions. Figure 9b shows that the increase in occurrence is still present both at noon and in the flank magnetosphere. We conclude that solar wind flow speed affects the occurrence rate of global modes at all frequencies, and that the effect may not be due solely to a preference for radial IMF conditions at higher solar wind flow speed. We cannot presently determine whether this increase occurs because more energy is available for global modes during these intervals or because of changes to the magnetosheath boundary. However, if the former is true, we expect that at least some of this energy must come directly from the solar wind, since surface waves driven by flow shear would be less likely to occur near noon, yet the occurrence rate is still observed to increase substantially in this sector.

4.5. Favored Driving Conditions for Global Modes—Solar Wind Dynamic Pressure

[78] Solar wind dynamic pressure fluctuations are an important energy source of ULF waves in the Earth's magnetosphere [e.g., *Kepko et al.*, 2002; *Takahashi and Ukhorskiy*, 2007], and they have been linked to global modes in several case studies [e.g., *Eriksson et al.*, 2006; *Hartinger et al.*, 2012]. Although these fluctuations can provide energy for global modes, they can also preclude their occurrence. *Kivelson et al.* [1997] noted that to grow, cavity modes, a type of global mode, require a cavity with stable dimensions, plasma parameters, and magnetic field configuration. Global modes in the magnetosphere are affected when the dimensions of the magnetosphere change, and solar wind dynamic pressure plays an important role in determining the dimensions of the magnetosphere—in particular, the magnetopause location [*Shue et al.*, 1997].

[79] Changes in solar wind dynamic pressure that are comparable to global mode periods can drive global modes [e.g., *Claudepierre et al.*, 2009], but they can also preclude their occurrence if the fluctuations are sufficiently large that they cause a significant change in the dimensions of the magnetospheric cavity. We demonstrate this with a 1-D model of a fast mode wave standing between two perfectly reflecting boundaries, one of which is the magnetopause. The inner boundary is at location r_0 and the outer boundary is at the magnetopause location, r. The fast magnetosonic speed, v_{fm} is uniform everywhere. The fundamental frequency of the standing fast mode wave is then

$$f = \frac{v_{fm}}{2(r - r_0)} \tag{1}$$

When the outer boundary is displaced by an amount Δr, the frequency changes by an amount

$$\Delta f = \frac{-v_{fm}\Delta r}{2(r - r_0)(r - r_0 + \Delta r)} \tag{2}$$

Equation (2) shows that the larger the displacement of the boundary, the larger the frequency change. It also shows that an inner, or negative, displacement of the boundary increases the frequency, whereas an outer displacement reduces the frequency, consistent with decrease or increase in the fast mode transit time as the boundary location changes. The absolute value of the frequency change can be compared to the original cavity frequency, assuming Δr is small compared to $r - r_0$, using

$$\frac{f}{|\Delta f|} \approx \frac{r - r_0}{|\Delta r|} \tag{3}$$

As the displacement of the boundary becomes larger relative to the original cavity size, the frequency change becomes larger relative to the original frequency.

[80] This 1-D model can be used to show qualitatively how the occurrence rate of global modes should depend on

changes in the boundary location in the magnetosphere due to solar wind dynamic pressure, with the understanding that other factors, such as the inner boundary condition, can also play a role in determining their occurrence. We consider the magnetopause location as the outer boundary and the equatorial ionosphere as the inner boundary (r_0 = 1 *Re*). Using the *Shue et al.* [1997] empirical model, the magnetopause location at the subsolar point when the z component of the IMF is 0 is

$$r = 11.4P^{\frac{-1}{6.6}} \quad (4)$$

where P is the solar wind dynamic pressure. To use equation (3), we also require an estimate of the displacements of the outer boundary due to dynamic pressure. *Takahashi and Ukhorskiy* [2007] showed that instantaneous measurements (1 min) of solar wind dynamic pressure and the amplitude of solar wind dynamic pressure fluctuations in the Pc5 frequency band are extremely well correlated. Using the results from Figure 14 in that study, we find that the relationship between them is given by

$$\delta P(Pc5) = 0.0026P^{1.89} \quad (5)$$

Using equations (3)–(5), we find the dependence of $(r - r_0)/\Delta r$ on the solar wind dynamic pressure based on the 1-D model for global mode frequencies in the mHz range (Pc5). Figure 10a shows how $(r - r_0)/\Delta r$ changes as a function of solar wind dynamic pressure (red line). In the absence of other effects, increasing the dynamic pressure will decrease $(r - r_0)/\Delta r$, or render the magnetospheric cavity/waveguide less effective at sustaining global modes. As $(r - r_0)/\Delta r$ decreases, the energy supplied to global modes by dynamic pressure fluctuations will increase, as indicated by equation (5) and the black line in Figure 10a. Although these two effects may both be important, one will tend to decrease the occurrence of global modes, whereas the other will increase it.

[81] Figure 10b shows the occurrence rate of global modes as a function of solar wind dynamic pressure. There is no significant difference between the occurrence rates in the first two bins, but the occurrence rate is significantly lower in the highest bin ($1.2 < P \leq 3.76$ nPa) compared to the first two bins. This is the opposite trend from what is expected for magnetospheric ULF waves directly driven by solar wind dynamic pressure fluctuations; the amplitude of these waves should and does increase as the amplitude of the dynamic pressure fluctuations increases [*Takahashi and Ukhorskiy*, 2007]. However, this trend is expected for global modes if the effect of $(r - r_0)/\Delta r$ decreasing with increasing dynamic pressure is more important than the increase in the energy supplied to global modes.

[82] This result is not inconsistent with the correlation between global mode occurrence and upstream wave activity (section 4.3). Upstream waves generate dynamic pressure fluctuations that could perturb the magnetopause, but their perturbation amplitudes are less than 20% of the perturbations in the pristine solar wind [*Le and Russell*, 1994; *Greenstadt et al.*, 1995]. Furthermore, their magnetopause perturbations ought to be more restricted in local time (consistent with the location of the quasi-parallel bow shock) than those generated by the pristine solar wind, so they would not necessarily preclude the occurrence of global modes at all local times. Finally, the amount of energy from upstream waves that ultimately penetrates the magnetosheath perturbs the magnetopause may be small [*Engebretson et al.*, 1991].

[83] The reduction in the occurrence rate at higher dynamic pressure values may also be partially caused by a biasing against intervals when global modes can be unambiguously identified: The presence of ULF wave activity, whether directly driven monochromatic ULF waves or waves with a broadband frequency spectrum, may be obscuring global modes during intervals when solar wind dynamic pressure fluctuations have larger amplitudes.

4.6. Favored Frequencies for Global Modes

[84] Global mode frequency depends on the properties of the magnetospheric cavity/waveguide. Cavity size will affect the frequency; for example, larger cavities will tend to have lower frequencies (equation (1)). The plasma conditions inside the cavity/waveguide also affect frequency; for example, a significant population of heavy ions will decrease it. Frequency can also be affected by boundary

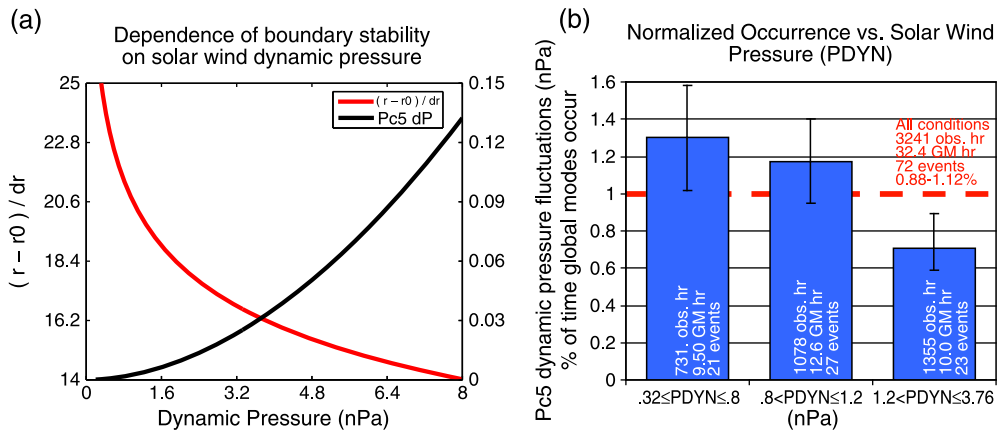

Figure 10. (a) The dependance of $(r - r_0)/\Delta r$, a measure of boundary stability, on solar wind dynamic pressure (red), and the dependence of solar wind dynamic pressure Pc5 fluctuation amplitude on solar wind dynamic pressure (black). (b) The occurrence rate of global mode events versus solar wind dynamic pressure.

conditions [*Mann et al.*, 1999]. It is noteworthy that more than one type of cavity/waveguide mode is possible; the equatorial ionosphere, plasmapause, magnetopause, and bow shock have all been proposed as potential cavity/waveguide mode boundaries, leading to a number of possible cavities, each having its own distinct frequency. Proposed and observed global mode frequencies have ranged from $\leq$ 1 mHz to tens of mHz [e.g., *Lee and Lysak*, 1989; *Kivelson et al.*, 1997; *Claudepierre et al.*, 2009].

[85] Given this wide range of possibilities for global mode frequency, it is difficult to predict exactly what trend, if any, should be expected when an ensemble of global mode observations at a range of radial distances and magnetic local times is examined. We have already demonstrated in Figure 8 that global modes with frequencies above 10 mHz are preferentially driven by the ion foreshock in the prenoon and noon local time sectors. This is consistent with reports from MHD simulations and observations of cavity mode frequencies in that region [*Kivelson et al.*, 1997; *Claudepierre et al.*, 2009]. However, these are not the only global mode frequencies that can be excited in that region, as evidenced by Figure 8a. The ion foreshock is only effective at driving global modes in that region when the driving frequency spectrum from the ion foreshock overlaps one or more of the accessible global mode frequencies in the magnetosphere [*Wright*, 1994]. These frequencies could correspond to a subset of possible cavity/waveguides in the dayside magnetosphere; the cavity/waveguides corresponding to the lower frequency global modes that were found on the dayside may be larger and may not be effectively driven by the ion foreshock.

[86] Figure 11 shows the frequency of all global mode events versus position in the GSM *xy* plane. Apart from the clustering of higher frequency ($10 < f \leq 20$ mHz) global modes on the dayside, there are no immediately obvious trends. The lower frequency ($3 \leq f \leq 10$ mHz) global modes occur at all local times and radial distances. Notably, they do not have decreasing frequencies with increasing radial distance. This trend would be expected for standing Alfvén waves, which nominally have decreasing frequencies with increasing radial distances in this region (outside the plasmasphere). The absence of this trend is further evidence that our methodology has selected global mode events rather than standing Alfvén waves.

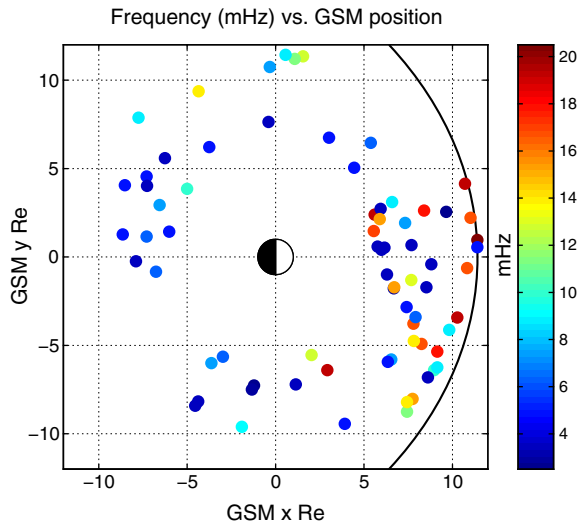

Figure 11. The position of each global mode event in the GSM *xy* plane. The global mode frequency (mHz) is indicated in color.

[87] The lack of a clear trend with respect to radial distance or magnetic local time or a preference for specific frequencies suggests that there is significant variability in the properties of magnetospheric cavities/waveguides. This is reasonable when considering the variability expected in, for example, the magnetopause location or the distribution of plasma mass density from event to event. We note here that we only searched for events in the frequency range $3 \leq f \leq 20$ mHz, and thus we cannot comment on global mode frequencies outside that range, such as the ULF waves observed on the ground at discrete frequencies below 3 mHz [*Samson et al.*, 1991]. In the frequency range we considered, we found that 36 out of 72 events had frequencies in the Pc5 frequency range, suggesting a preference for Pc5 frequencies in the region we considered (radial distance greater than 5 Re). There was no statistically significant preference for global modes to occur at discrete frequencies. However, it is possible that with more events such trends could be identified.

[88] To summarize, global modes with frequencies between 10 and 20 mHz occur almost exclusively on the dayside. Those with frequencies in the range $3 \leq f \leq 10$ mHz occur at all local times and radial distances considered in this study ($5 < r \leq 13$ Re), with no clear frequency trends evident. Half of the global modes in our database had frequencies in the Pc5 frequency range.

5. Summary

[89] We used data from multiple THEMIS spacecraft to identify 72 global mode events. Our event selection criteria were designed to use magnetic field, electric field, and plasma data from a single probe as well as multi-probe and ground observations to identify these global modes while excluding other ULF wave modes. This is the first study to identify a large number of global modes using in situ wave mode identification, providing strong evidence for the existence of global modes outside the plasmasphere. It also provides an opportunity to study the the behavior of global modes in aggregate, something not possible in case studies.

[90] Using an ensemble of 72 events (listed in Supporting Information, Table S1), we characterized the behavior of global modes, obtaining a lower bound of 1.0% for their overall occurrence rate in the Earth's magnetosphere. We also found that global modes are more likely to occur in the noon local time sector and at radial distances less than 7.5 *Re*. The ion foreshock is an important source of energy for global modes with frequencies greater than 10 mHz, and the occurrence of all global modes generally increases with increasing solar wind flow speed and decreasing solar wind dynamic pressure. Half of the global modes we identified had frequencies in the Pc5 range.

[91] After visually inspecting band-pass-filtered data from each event, we found that only 10 global mode events out of 72 had magnetic field *z* perturbations greater than 1 nT. Although our study may be biased to observe lower

amplitude global modes (see section 3.4), it is noteworthy that so many events in the database had low wave amplitudes compared to other ULF wave modes generated during nominal or geomagnetically active conditions [*Zhu and Kivelson*, 1991]. These low amplitudes would make it difficult to identify global modes in the presence of other ULF wave modes with similar frequencies, perhaps explaining the paucity of in situ global mode observations.

[92] Global modes, regardless of whether they have low amplitudes, can play an important role in driving standing Alfvén waves, which can have significant amplitudes, as shown in previous models and observations [*Kivelson and Southwood*, 1985; *Hartinger et al.*, 2012]. Thus, they are a viable mechanism for coupling energy from the solar wind into the magnetosphere and ionosphere (via Alfvén waves), and this study suggests that they may occur more frequently than previously thought. Studying the importance of global modes relative to other energy transfer mechanisms is a topic for future work.

[93] In light of these results, we suggest two possibilities for future studies using multi-spacecraft observations to advance the understanding of wave mode coupling in the Earth's magnetosphere. A study that uses statistical analysis with simultaneous observations at the magnetopause, in the magnetosphere, and on the ground could examine the response of the magnetosphere to magnetopause surface waves or pulses; in particular, the excitation of standing Alfvén waves. This study could be used to determine whether global modes routinely play a role in wave mode coupling with shear Alfvén waves and whether they are an important mechanism for coupling energy from the solar wind to the magnetosphere and ionosphere. A second study that uses statistical analysis with routine identification of waveguide modes using azimuthally separated spacecraft (as in *Mann et al.* [1998]) or with ground observations (as in *Mathie and Mann* [2000]) could be used to obtain a nominal occurrence rate for global modes rather than a lower bound, as in this study.

[94] **Acknowledgments.** We acknowledge NASA THEMIS contract NAS5-02099 and thank C. W. Carlson and J. P. McFadden for the use of the ESA data, D. Larson and R. P. Lin for the use of SST data, and J. W. Bonnell and F. S. Mozer for use of EFI data. We thank the NASA Space Science Data facility for use of solar wind data and geomagnetic activity indices. The work done by Mark B. Moldwin was supported by NASA grant NNXAI626. The work done by Kazue Takahashi was supported by NSF grant ATM-0750689. We thank Margaret Kivelson, David Sibeck, and Ferdinand Plaschke for useful discussions.

References

Anderson, B. J. (1993), Statistical studies of Pc 3-5 pulsations and their relevance for possible source mechanisms of ULF waves, *Ann. Geophys.*, *11*, 128–143.

Anderson, B. J., and M. J. Engebretson (1995), Relative intensity of toroidal and compressional Pc 3-4 wave power in the dayside outer magnetosphere, *J. Geophys. Res.*, *100*, 9591–9604.

Anderson, B. J., M. J. Engebretson, and L. J. Zanetti (1989), Distortion effects in spacecraft observations of MHD toroidal standing waves—Theory and observations, *J. Geophys. Res.*, *94*, 13,425–13,445.

Auster, H. U., et al. (2008), The THEMIS fluxgate magnetometer, *Space Sci. Rev.*, *141*, 235–264, doi:10.1007/s11214-008-9365-9.

Baumjohann, W., N. Sckopke, J. Labelle, B. Klecker, and H. Luehr (1987), Plasma and field observations of a compressional Pc 5 wave event, *J. Geophys. Res.*, *92*, 12,203–12,212.

Bonnell, J. W., F. S. Mozer, G. T. Delory, A. J. Hull, R. E. Ergun, C. M. Cully, V. Angelopoulos, and P. R. Harvey (2008), The electric field instrument (EFI) for THEMIS, *Space Sci. Rev.*, *141*, 303–341, doi: 10.1007/s11214-008-9469-2.

Burgess, D. (1997), What do we really know about upstream waves? *Adv. Space Res.*, *20*, 673–682.

Chen, L., and A. Hasegawa (1974), A theory of long-period magnetic pulsations, 1. Steady state excitation of field line resonance, *J. Geophys. Res.*, *79*, 1024–1032.

Chi, P. J., and C. T. Russell (1998), Phase skipping and Poynting flux of continuous pulsations, *J. Geophys. Res.*, *103*, 29,479–29,492.

Claudepierre, S. G., M. Wiltberger, S. R. Elkington, W. Lotko, and M. K. Hudson (2009), Magnetospheric cavity modes driven by solar wind dynamic pressure fluctuations, *Geophys. Res. Lett.*, *36*, L13101, doi: 10.1029/2009GL039045.

Clausen, L. B. N., and T. K. Yeoman (2009), Comprehensive survey of Pc4 and Pc5 band spectral content in Cluster magnetic field data, *Ann. Geophys.*, *27*, 3237–3248, doi:10.5194/angeo-27-3237-2009.

Clausen, L. B. N., T. K. Yeoman, R. C. Fear, R. Behlke, E. A. Lucek, and M. J. Engebretson (2009), First simultaneous measurements of waves generated at the bow shock in the solar wind, the magnetosphere and on the ground, *Ann. Geophys.*, *27*, 357–371, doi:10.5194/angeo-27-357-2009.

Eastwood, J. P., S. J. Schwartz, T. S. Horbury, C. M. Carr, K.-H. Glassmeier, I. Richter, C. Koenders, F. Plaschke, and J. A. Wild (2011), Transient Pc3 wave activity generated by a hot flow anomaly: Cluster, Rosetta, and ground-based observations, *J. Geophys. Res.*, *116*(A15), A08224, doi:10.1029/2011JA016467.

Engebretson, M. J., L. J. Zanetti, T. A. Potemra, and M. H. Acuna (1986), Harmonically structured ULF pulsations observed by the AMPTE CCE magnetic field experiment, *Geophys. Res. Lett.*, *13*, 905–908.

Engebretson, M. J., N. Lin, W. Baumjohann, H. Luehr, and B. J. Anderson (1991), A comparison of ULF fluctuations in the solar wind, magnetosheath, and dayside magnetosphere. I—Magnetosheath morphology. II—Field and plasma conditions in the magnetosheath, *J. Geophys. Res.*, *96*, 3441–3464.

Eriksson, P. T. I., L. G. Blomberg, S. Schaefer, and K.-H. Glassmeier (2006), On the excitation of ULF waves by solar wind pressure enhancements, *Ann. Geophys.*, *24*, 3161–3172, doi: 10.5194/angeo-24-3161-2006.

Fairfield, D. H., W. Baumjohann, G. Paschmann, H. Luehr, and D. G. Sibeck (1990), Upstream pressure variations associated with the bow shock and their effects on the magnetosphere, *J. Geophys. Res.*, *95*, 3773–3786.

Frey, S., V. Angelopoulos, M. Bester, J. Bonnell, T. Phan, and D. Rummel (2008), Orbit design for the THEMIS mission, *Space Sci. Rev.*, *141*, 61–89, doi:10.1007/s11214-008-9441-1.

Greenstadt, E. W., G. Le, and R. J. Strangeway (1995), ULF waves in the foreshock, *Adv. Space Res.*, *15*, 71–84.

Hartinger, M., V. Angelopoulos, M. B. Moldwin, Y. Nishimura, D. L. Turner, K.-H. Glassmeier, M. G. Kivelson, J. Matzka, and C. Stolle (2012), Observations of a Pc5 global (cavity/waveguide) mode outside the plasmasphere by THEMIS, *J. Geophys. Res.*, *117* (A16), A06202, doi:10.1029/2011JA017266.

Hasegawa, A. (1969), Drift mirror instability of the magnetosphere, *Phys. Fluids*, *12*, 2642–2650.

Kepko, L., and H. E. Spence (2003), Observations of discrete, global magnetospheric oscillations directly driven by solar wind density variations, *J. Geophys. Res.*, *108*, 1257, doi:10.1029/2002JA009676.

Kepko, L., H. E. Spence, and H. J. Singer (2002), ULF waves in the solar wind as direct drivers of magnetospheric pulsations, *Geophys. Res. Lett.*, *29*(8), 1197, doi:10.1029/2001GL014405.

Kim, H.-J., L. Lyons, A. Boudouridis, V. Pilipenko, A. J. Ridley, and J. M. Weygand (2011), Statistical study of the effect of ULF fluctuations in the IMF on the cross polar cap potential drop for northward IMF, *J. Geophys. Res.*, *116*(A15), A10311.

Kivelson, M. G., and D. J. Southwood (1985), Resonant ULF waves—A new interpretation, *Geophys. Res. Lett.*, *12*, 49–52.

Kivelson, M. G., and D. J. Southwood (1988), Hydromagnetic waves and the ionosphere, *Geophys. Res. Lett.*, *15*, 1271–1274.

Kivelson, M. G., J. Etcheto, and J. G. Trotignon (1984), Global compressional oscillations of the terrestrial magnetosphere—The evidence and a model, *J. Geophys. Res.*, *89*, 9851–9856.

Kivelson, M., M. Cao, R. McPherron, and R. Walker (1997), A possible signature of magnetic cavity mode oscillations in ISEE spacecraft observations, *J. Geomag. Geoelec.*, *49*(9), 1079–1098.

Le, G., and C. T. Russell (1994), The morphology of ULF waves in the Earth's foreshock, in *Washington DC American Geophysical Union Geophysical Monograph Series*, edited by Engebretson, M. J., K. Takahashi, and M. Scholer, vol. 81, 87 pp.

Lee, D.-H. (1998), On the generation mechanism of Pi 2 pulsations in the magnetosphere, *Geophys. Res. Lett.*, *25*, 583–586.

Lee, D.-H., and R. L. Lysak (1989), Magnetospheric ULF wave coupling in the dipole model—The impulsive excitation, *J. Geophys. Res.*, *94*, 17,097–17,103.

Lee, D.-H., and R. L. Lysak (1999), MHD waves in a three-dimensional dipolar magnetic field: A search for Pi2 pulsations, *J. Geophys. Res.*, *104*, 28,691–28,700.

Lessard, M. R., M. K. Hudson, and H. Lühr (1999), A statistical study of Pc3-Pc5 magnetic pulsations observed by the AMPTE/Ion Release Module satellite, *J. Geophys. Res.*, *104*, 4523–4538.

Love, J. J., and C. A. Finn (2011), The USGS geomagnetism program and its role in space weather monitoring, *Space Weather*, *9*, S07001, doi: 10.1029/2001GL014405.

Mann, I. R. (1997), On the internal radial structure of field line resonances, *J. Geophys. Res.*, *102*, 27,109–27,120.

Mann, I. R., G. Chisham, and S. D. Bale (1998), Multisatellite and ground-based observations of a tailward propagating Pc5 magnetospheric waveguide mode, *J. Geophys. Res.*, *103*, 4657–4670.

Mann, I. R., A. N. Wright, K. J. Mills, and V. M. Nakariakov (1999), Excitation of magnetospheric waveguide modes by magnetosheath flows, *J. Geophys. Res.*, *104*, 333–354.

Mann, I. R., et al. (2008), The upgraded CARISMA magnetometer array in the THEMIS era, *Space Sci. Rev.*, *141*, 413–451, doi:10.1007/s11214-008-9457-6.

Mathie, R. A., and I. R. Mann (2000), Observations of Pc5 field line resonance azimuthal phase speeds: A diagnostic of their excitation mechanism, *J. Geophys. Res.*, *105*, 10,713–10,728.

McFadden, J. P., C. W. Carlson, D. Larson, M. Ludlam, R. Abiad, B. Elliott, P. Turin, M. Marckwordt, and V. Angelopoulos (2008), The THEMIS ESA plasma instrument and in-flight calibration, *Space Sci. Rev.*, *141*, 277–302, doi:10.1007/s11214-008-9440-2.

McIlwain, C. E. (1966), Magnetic coordinates, *Space Sci. Rev.*, *5*, 585–598.

Moldwin, M. B., L. Downward, H. K. Rassoul, R. Amin, and R. R. Anderson (2002), A new model of the location of the plasmapause: CRRES results, *J. Geophys. Res. (Space Phys.)*, *107*(A11), 1339, doi: 10.1029/2001JA009211.

Paschmann, G., and P. W. Daly (2000), *Analysis Methods for Multi-Spacecraft Data*, ESA Publications Division.

Piersanti, M., U. Villante, C. Waters, and I. Coco (2012), The 8 June 2000 ULF wave activity: A case study, *J. Geophys. Res.*, *117*(A16), A02204, doi:10.1029/2011JA016857.

Pokhotelov, O. A., V. A. Pilipenko, and E. Amata (1985), Drift anisotropy instability of a finite-beta magnetospheric plasma, *Planet. Space Sci.*, *33*, 1229–1241.

Radoski, H. R. (1971), A note on the problem of hydromagnetic resonances in the magnetosphere, *Planet. Space Sci.*, *19*, 1012–1013.

Rickard, G. J., and A. N. Wright (1995), ULF pulsations in a magnetospheric waveguide: Comparison of real and simulated satellite data, *J. Geophys. Res.*, *100*, 3531–3537.

Russell, C. T., P. J. Chi, D. J. Dearborn, Y. S. Ge, B. Kuo-Tiong, J. D. Means, D. R. Pierce, K. M. Rowe, and R. C. Snare (2008), THEMIS ground-based magnetometers, *Space Sci. Rev.*, *141*, 389–412, doi: 10.1007/s11214-008-9337-0.

Samson, J. C., and G. Rostoker (1972), Latitude-dependent characteristics of high-latitude Pc 4 and Pc 5 micropulsations, *J. Geophys. Res.*, *77*, 6133–6144.

Samson, J. C., R. A. Greenwald, J. M. Ruohoniemi, T. J. Hughes, and D. D. Wallis (1991), Magnetometer and radar observations of magnetohydrodynamic cavity modes in the Earth's magnetosphere, *Can. J. Phys.*, *69*, 929–937.

Samson, J. C., B. G. Harrold, J. M. Ruohoniemi, R. A. Greenwald, and A. D. M. Walker (1992), Field line resonances associated with MHD waveguides in the magnetosphere, *Geophys. Res. Lett.*, *19*, 441–444.

Sciffer, M. D., C. L. Waters, and F. W. Menk (2005), A numerical model to investigate the polarisation azimuth of ULF waves through an ionosphere with oblique magnetic fields, *Ann. Geophys.*, *23*, 3457–3471, doi:10.5194/angeo-23-3457-2005.

Shue, J.-H., J. K. Chao, H. C. Fu, C. T. Russell, P. Song, K. K. Khurana, and H. J. Singer (1997), A new functional form to study the solar wind control of the magnetopause size and shape, *J. Geophys. Res.*, *102*, 9497–9512.

Sibeck, D. G., and V. Angelopoulos (2008), THEMIS science objectives and mission phases, *Space Sci. Rev.*, *141*, 35–59, doi:10.1007/s11214-008-9393-5.

Song, P., C. T. Russell, and S. P. Gary (1994), Identification of low-frequency fluctuations in the terrestrial magnetosheath, *J. Geophys. Res.*, *99*, 6011–6025, doi:10.1029/93JA03300.

Southwood, D. J. (1974), Some features of field line resonances in the magnetosphere, *Planet. Space Sci.*, *22*, 483–491.

Southwood, D. J. (1977), Localised compressional hydromagnetic waves in the magnetospheric ring current, *Planet. Space Sci.*, *25*, 549–554.

Takahashi, K., R. L. McPherron, E. W. Greenstadt, and C. A. Neeley (1981), Factors controlling the occurrence of Pc 3 magnetic pulsations at synchronous orbit, *J. Geophys. Res.*, *86*, 5472–5484.

Takahashi, K., R. L. McPherron, and T. Terasawa (1984), Dependence of the spectrum of Pc 3-4 pulsations on the interplanetary magnetic field, *J. Geophys. Res.*, *89*, 2770–2780.

Takahashi, K., D.-H. Lee, M. Nosé, R. R. Anderson, and W. J. Hughes (2003), CRRES electric field study of the radial mode structure of Pi2 pulsations, *J. Geophys. Res.*, *108*, 1210, doi:10.1029/2002JA009761.

Takahashi, K., and A. Y. Ukhorskiy (2007), Solar wind control of Pc5 pulsation power at geosynchronous orbit, *J. Geophys. Res. (Space Phys.)*, *112*(A11), A11205, doi:10.1029/2007JA012483.

Takahashi, K., et al. (2010), Multipoint observation of fast mode waves trapped in the dayside plasmasphere, *J. Geophys. Res.*, *115* (A14), A12247, doi:10.1029/2010JA015956.

Tamao, T. (1965), Transmission and coupling resonance of hydromagnetic disturbances in the non-uniform Earth's magnetosphere, *Tohoku University, Science Reports, Series 5, Geophysics (2)*, *17*, 43–72.

Troitskaya, V. A., T. A. Plyasova-Bakunina, and A. V. Gul'Elmi (1971), The connection of Pc2-4 pulsations with the interplanetary magnetic field, *Akademiia Nauk SSSR Doklady*, *197*, 1312–1314.

Turner, D. L., Y. Shprits, M. Hartinger, and V. Angelopoulos (2012), Explaining sudden losses of outer radiation belt electrons during geomagnetic storms, *Nature Phys*, *8*, 208–212, doi:10.1038/NPHYS2185.

Viall, N. M., L. Kepko, and H. E. Spence (2009), Relative occurrence rates and connection of discrete frequency oscillations in the solar wind density and dayside magnetosphere, *J. Geophys. Res.*, *114*(A13), A01201, doi: 10.1029/2008JA013334.

Waters, C. L., J. C. Samson, and E. F. Donovan (1995), The temporal variation of the frequency of high latitude field line resonances, *J. Geophys. Res.*, *100*, 7987–7996.

Waters, C. L., K. Takahashi, D.-H. Lee, and B. J. Anderson (2002), Detection of ultralow-frequency cavity modes using spacecraft data, *J. Geophys. Res.*, *107*, 1284, doi:10.1029/2001JA000224.

Wright, A. N. (1994), Dispersion and wave coupling in inhomogeneous MHD waveguides, *J. Geophys. Res.*, *99*, 159–167.

Wright, A. N., and G. J. Rickard (1995), A numerical study of resonant absorption in a magnetohydrodynamic cavity driven by a broadband spectrum, *Astrophys. J.*, *444*, 458–470.

Yeoman, T. K., D. M. Wright, T. R. Robinson, J. A. Davies, and M. Rietveld (1997), High spatial and temporal resolution observations of an impulse-driven field line resonance in radar backscatter artificially generated with the Tromsø heater, *Ann. Geophys.*, *15*, 634–644.

Zhu, X., and M. G. Kivelson (1989), Global mode ULF pulsations in a magnetosphere with a nonmonotonic Alfven velocity profile, *J. Geophys. Res.*, *94*, 1479–1485.

Zhu, X., and M. G. Kivelson (1991), Compressional ULF waves in the outer magnetosphere. I—Statistical study, *J. Geophys. Res.*, *96*(19), 451.